AGU PUBLICATIONS

Global Biogeochemical Cycles

RESEARCH ARTICLE
10.1002/2016GB005415

Key Points:
- Nitrate and nitrite isotopes can be used in inverse 1-D modeling to predict rates of nitrogen cycle processes in ODZs
- Close coupling of nitrate reduction and nitrite oxidation is suggested by model results
- Tighter constraints on isotope effects for nitrate reduction and nitrite oxidation are greatly needed

Supporting Information:
- Supporting Information S1
- Text S1

Correspondence to:
B. D. Peters and K. L. Casciotti,
bpeters1@stanford.edu;
kcasciotti@stanford.edu

Citation:
Peters, B. D., A. R. Babbin, K. A. Lettmann, C. W. Mordy, O. Ulloa, B. B. Ward, and K. L. Casciotti (2016), Vertical modeling of the nitrogen cycle in the eastern tropical South Pacific oxygen deficient zone using high-resolution concentration and isotope measurements, *Global Biogeochem. Cycles*, *30*, 1661–1681, doi:10.1002/2016GB005415.

Received 19 MAR 2016
Accepted 3 OCT 2016
Accepted article online 15 OCT 2016
Published online 10 NOV 2016

Vertical modeling of the nitrogen cycle in the eastern tropical South Pacific oxygen deficient zone using high-resolution concentration and isotope measurements

Brian D. Peters[1], Andrew R. Babbin[2,3], Karsten A. Lettmann[4], Calvin W. Mordy[5,6], Osvaldo Ulloa[7], Bess B. Ward[2], and Karen L. Casciotti[1]

[1]Department of Earth System Science, Stanford University, Stanford, California, USA, [2]Department of Geosciences, Princeton University, Princeton, New Jersey, USA, [3]Department of Civil and Environmental Engineering, Massachusetts Institute of Technology, Cambridge, Massachusetts, USA, [4]Institute for Chemistry and Biology of the Sea, Oldenburg University, Oldenburg, Germany, [5]Joint Institute for the Study of the Atmosphere and Ocean, University of Washington, Seattle, Washington, USA, [6]Pacific Marine Environmental Laboratory, National Oceanic and Atmospheric Administration, Seattle, Washington, USA, [7]Departamento de Oceanografía and Instituto Milenio de Oceanografía, Universidad de Concepción, Concepción, Chile

Abstract Marine oxygen deficient zones (ODZs) have long been identified as sites of fixed nitrogen (N) loss. However, the mechanisms and rates of N loss have been debated, and traditional methods for measuring these rates are labor-intensive and may miss hot spots in spatially and temporally variable environments. Here we estimate rates of heterotrophic nitrate reduction, heterotrophic nitrite reduction (denitrification), nitrite oxidation, and anaerobic ammonium oxidation (anammox) at a coastal site in the eastern tropical South Pacific (ETSP) ODZ based on high-resolution concentration and natural abundance stable isotope measurements of nitrate (NO_3^-) and nitrite (NO_2^-). These measurements were used to estimate process rates using a two-step inverse modeling approach. The modeled rates were sensitive to assumed isotope effects for NO_3^- reduction and NO_2^- oxidation. Nevertheless, we addressed two questions surrounding the fates of NO_2^- in the ODZ: (1) Is NO_2^- being primarily reduced to N_2 or oxidized to NO_3^- in the ODZ? and (2) what are the contributions of anammox and denitrification to NO_2^- removal? Depth-integrated rates from the model suggest that 72–88% of the NO_2^- produced in the ODZ was oxidized back to NO_3^-, while 12–28% of NO_2^- was reduced to N_2. Furthermore, our model suggested that 36–74% of NO_2^- loss was due to anammox, with the remainder due to denitrification. These model results generally agreed with previously measured rates, though with a large range of uncertainty, and they provide a long-term integrated view that compliments incubation experiments to obtain a broader picture of N cycling in ODZs.

1. Introduction

Nitrogen (N) is thought to be a limiting nutrient in large expanses of the open ocean [*Boynton et al*., 1982; *Codispoti*, 1989; *Tyrell*, 1999]. Most marine organisms can readily take up N in the forms of nitrate (NO_3^-), nitrite (NO_2^-), and ammonium (NH_4^+), which are collectively known as "fixed N," but nitrogen gas (N_2) can only be utilized by a subset of marine organisms known as "diazotrophs." Marine oxygen deficient zones (ODZs) have long been identified as regions important for control of the fixed N budget [*Thomas*, 1966; *Cline and Richards*, 1972; *Codispoti and Christensen*, 1985], where fixed N is converted into gaseous N_2 under low oxygen (O_2) conditions, thus becoming biologically unavailable to most marine organisms (save for the diazotrophs). While some have identified the upper concentrations of O_2 allowing fixed N loss as 4–5 μmol/kg [*Paulmier and Ruiz-Pino*, 2009], recent advances in [O_2] measurement technology have revealed that these processes may be inhibited by dissolved [O_2] as low as 10 nmol kg^{-1}, the detection limit for the switchable trace oxygen ("STOX") sensor [*Revsbech et al*., 2009; *Thamdrup et al*., 2012; *Ulloa et al*., 2012; *Tiano et al*., 2014; *Dalsgaard et al*., 2014].

Some previous studies have proposed that ODZs are likely to expand in a warmer climate [*Stramma et al*., 2008; *Keeling et al*., 2010], though a recent study has found evidence for contraction of ODZs [*Deutsch et al*., 2014]. The volume and areal extent of regions with nanomolar [O_2] directly affects the marine N budget, as dissolved [O_2] controls the physical domain where fixed N can be converted to N_2. Resolving the magnitude and mechanisms of fixed N cycling and loss in ODZs will be crucial to understanding the biogeochemical impacts of and feedbacks on changes in ODZ area and volume.

One of the most prominent characteristics of marine ODZs is the accumulation of NO_2^- in suboxic waters, a feature known as the secondary NO_2^- maximum (SNM). Thought to be produced by dissimilatory NO_3^- reduction [*Brandhorst*, 1959; *Thomas*, 1966; *Goering*, 1968; *Cline and Richards*, 1972; *Lam et al*., 2011], NO_2^- represents a key "branch point" in the marine N cycle, as it can either be reduced to N_2 via denitrification or anammox [*Cline and Richards*, 1972; *Codispoti and Richards*, 1976; *Strous et al*., 1998; *Thamdrup et al*., 2006; *Dalsgaard et al*., 2012], reduced via dissimilatory NO_3^- reduction to NH_4^+ ("DNRA") [*Lam et al*., 2009], or it can be oxidized back to NO_3^- via anammox or NO_2^--oxidizing bacteria [*Anderson et al*., 1982; *Ward et al*., 1989; *Lipschultz et al*., 1990]. Reduction to N_2 leads to fixed N "loss," while NO_2^- oxidation to NO_3^- and DNRA retain N in a fixed form. Thus, understanding the mechanisms of NO_2^- consumption is important for quantifying past and future changes in the marine N budget.

The most common way to measure the rates of these processes is through isotope tracer experiments. These incubation-based experiments involve collecting water from specific depths, amending the water with a heavy isotope enriched substrate (usually in the form of 99% ^{15}N), and measuring the heavy isotope enrichment of the product(s) over time. These methods have been employed to measure rates of NO_3^- reduction, denitrification, anammox, NO_2^- oxidation, and DNRA in ODZs with substantial success [*Ward et al*., 1989; *Lipschultz et al*., 1990; *Hamersley et al*., 2007; *Lam et al*., 2011; *Fussel et al*., 2012; *Kalvelage et al*., 2013; *Babbin et al*., 2014]. However, measuring the rates of these biogeochemical processes with on-deck incubation experiments is very labor intensive and has proven to be a challenge, primarily due to the O_2 sensitivity of the processes in question and the difficulties of maintaining an O_2-free incubation environment [*Dalsgaard et al*., 2003; *Shosky*, 2005; *Kalvelage et al*., 2011; *De Brabandere et al*., 2012; *Dalsgaard et al*., 2014]. Additionally, the bottle enclosure and addition of substrate during these experiments may inhibit or stimulate these processes, resulting in unrepresentative rate measurements. Finally, natural spatial and temporal variability of N cycle transformations can lead to difficulty in extrapolating point measurements over appropriate space and time scales. Natural abundance isotope samples, on the other hand, are integrative measurements that reflect the accumulated effects of N cycle processes over larger scales of time and space.

Interpretations of natural abundance isotope measurements make use of the fact that biogeochemical processes change the ratios of ^{15}N to ^{14}N in NO_3^- and NO_2^- (reported as $\delta^{15}N$ in units of per mil (‰), where $\delta^{15}N = [(^{15}N/^{14}N)_{sample} \div (^{15}N/^{14}N)_{reference} - 1] \times 10^3$). This isotopic fractionation arises from a difference in the reaction rate constant for ^{15}N (^{15}k) and that of ^{14}N (^{14}k) that varies among biogeochemical processes. The fractionation factor, α, for a given process is given by ($^{14}k/^{15}k$) and the isotope effect, ε, by $(\alpha - 1) \times 10^3$ in units of per mil (‰) [*Mariotti et al*., 1981]. For normal kinetic isotope fractionation, ^{14}k will be larger than ^{15}k, and thus $\alpha > 1$ and $\varepsilon > 0$. For inverse isotope fractionation, ^{14}k is lower than ^{15}k ($\alpha < 1$) and $\varepsilon < 0$. One can use known isotopic effects to interpret natural abundance isotope measurements of NO_2^- and NO_3^- and help disentangle the N cycle processes that have influenced N isotope distributions in a water parcel.

In interpreting the nutrient and isotope distributions, one must also account for the effects of physical processes such as mixing and advection, which play an important role in setting NO_3^- and NO_2^- concentration and isotope distributions in the ODZ regions [*Codispoti and Richards*, 1976; *Liu and Kaplan*, 1989; *Brandes et al*., 1998; *Voss et al*., 2001; *Casciotti et al*., 2013; *Bourbonnais et al*., 2015], particularly along density horizons [*Luyten et al*., 1983; *Warner and Weiss*, 1992; *Ledwell et al*., 1993]. In regions of coastal upwelling, such as Peru and Chile, vertical advection also constitutes an important upward flux of nutrients [*Chavez and Messie*, 2009] and vertical diffusion can operate when vertical nutrient gradients are strong [*Anderson et al*., 1982; *Lam et al*., 2011; *Banyte et al*., 2012]. Sharp gradients in [NO_3^-] and [NO_2^-] are observed toward the base of the oxycline in most ODZ environments, which should result in a vertical diffusive flux of these nutrients. In order for the characteristic ODZ features to be maintained, biological production and consumption must counteract physical transport.

In this study, we collected samples from two sites within the ETSP ODZ at high (~8 m) vertical resolution for stable isotope and concentration measurements of NO_2^- and NO_3^- using a pump profiling system (PPS). Data from one of the sites were analyzed in a steady state 1-D vertical advection-diffusion-reaction inverse model (Rate Estimation from Concentration (REC) model) [*Lettmann et al*., 2012], in order to obtain net rates of biological production or consumption of NO_3^- and NO_2^- in the ODZ in the absence of horizontal transport. These net rates were then decomposed into rates of dissimilatory NO_3^- reduction, denitrification (NO_2^- reduction), NO_2^- oxidation, and anammox required to balance steady state mass and isotope budgets

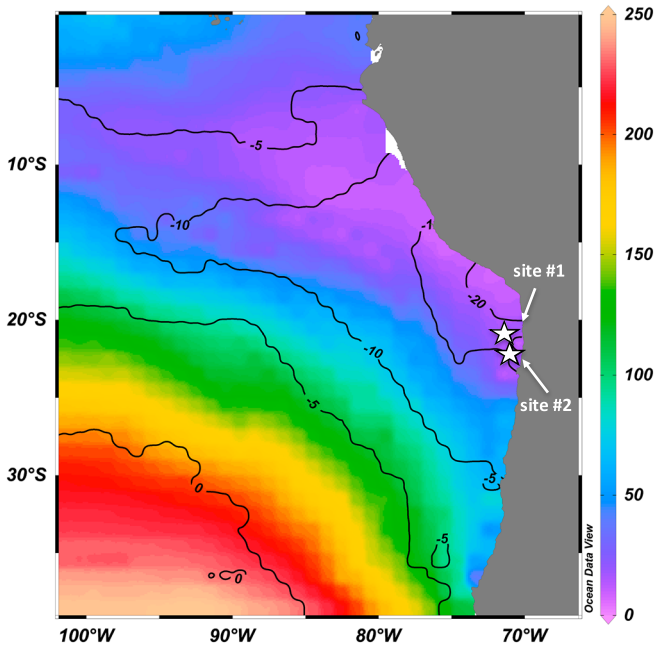

Figure 1. Shading indicates concentrations of dissolved oxygen along $\sigma_0 = 26.4$ kg m^{-3}, and contours give N* (N* = [NO_3^-] − 16 × [PO_4^{3-}] + 2.9 μmol kg^{-1}) along the same density surface. Data was obtained from World Ocean Atlas 2013 (note that [NO_2^-] data are not available in WOA13, and [NO_2^-] is thus not included in the calculations of N* shown here). The locations of the pump sites included in this study are indicated by stars. Nutrient and isotope measurements were collected at both sites, but only pump site #1 was used in the modeling exercise.

at regular depth intervals throughout the ODZ. Finally, we used the depth-integrated rates of these processes to estimate (1) the fraction of NO_2^- that is oxidized to NO_3^- in the ODZ and (2) the relative contributions of anammox and denitrification to NO_2^- removal (and N_2 production) in the ODZ. The rates of the processes included in the model are sensitive to the assumed isotope effects for NO_3^- reduction and NO_2^- oxidation. Accordingly, the model yielded a fairly large range of the fractions of NO_2^- oxidized and the relative contributions of anammox and denitrification. However, distinct trends were identified in N cycling between the upper and lower ODZ, as well as between different isotope effect scenarios, and these are discussed accordingly. Lastly, incubation-based rate measurements were also conducted at one of our two sites (A. R. Babbin et al., submitted, 2016). Comparison between the measured rates and the model output provides insights into the strengths and weaknesses of these approaches.

2. Materials and Methods

2.1. Study Site Description

Samples for this study were collected from two coastal sites in the ETSP in July 2013, which happened to coincide with a weak La Niña. This highly productive region has been studied extensively over the past 40 years, as Peruvian and Chilean coastlines are home to rich fisheries, and have proven to be relatively sensitive to seasonal changes, as well as changes in El Niño/La Niña state [*Barber and Chavez*, 1983; *Ulloa et al*., 2001; *Escribano et al*., 2004]. The ETSP is also home to a large permanent ODZ, where O_2 is depleted at middepth due to respiration of sinking organic matter and weak zonal currents that do not adequately resupply O_2 [*Wyrtki*, 1962; *Paulmier et al*., 2006; *Karstensen et al*., 2008; *Stramma et al*., 2010; *Czeschel et al*., 2011]. The focus of the study was site #1 (20.53°S, 70.71°W), which was located within the ETSP coastal upwelling regime (Figure 1) [*Wyrtki*, 1967; *Kessler*, 2006; *Pennington et al*., 2006]. Site #2, located at 21.50°S, 70.58°W, was investigated for comparison of NO_3^- and NO_2^- isotope distributions but not used in the model exercise due to the absence of in situ rate measurements for comparison. We note that pump site #2 had concentration and isotope profiles (Figure S1 in the supporting information) similar to pump site #1.

2.2. Concentration and Isotope Analysis

Samples for measurements of [NO_2^-], [NO_3^-], and [NH_4^+] were collected in 30 mL acid washed, high-density polyethylene bottles from both casts of the PPS (supporting information). These samples were analyzed shipboard shortly after collection using a custom autoanalyzer. WOCE-JGOFS protocols [*Gordon et al*., 2000] were followed for standardization and analysis, including reagent preparation, calibration of lab ware, preparation of primary and secondary standards, and corrections for blanks and refractive index. Measurements of [NO_3^- + NO_2^-] and [NO_2^-] were made using a modification of the red azo dye method [*Armstrong et al*., 1967; *Wood et al*., 1967], and measurements of [NH_4^+] used a modification of the indophenol blue method

[*Slawyk and MacIsaac*, 1972; *Mantoura and Woodward*, 1983; *Environmental Protection Agency*, 1984]. Detection limits of these measurements were not determined on this cruise, but the coefficient of variation (or CV) was determined by replicate analyses. For measurements of $[NO_3^-] > 10\ \mu M$, the CV was 0.08. For measurements of $[NO_2^-] > 1\ \mu M$, the CV was 0.007. $[NH_4^+]$ remained $< 0.1\ \mu M$ throughout the ODZ, and the CV was 0.07.

Water samples for NO_2^- and NO_3^- isotopic analysis were collected from the PPS in a 60 mL syringe, filtered through a 0.22 μm pore size Sterivex cartridge, and stored in 60 mL high-density polyethylene bottles. Subsamples were removed for preservation of N and O isotopes of NO_2^- on board, while the remaining sample was placed in a −20°C freezer and stored frozen for NO_3^- isotope analysis at Stanford University. Subsamples for NO_2^- isotope analyses were taken at depths where $[NO_2^-] > 0.3\ \mu M$, which was restricted to the depth range between ~82 m and 369 m. These samples were stored as N_2O after treatment with sodium azide [*McIlvin and Altabet*, 2005]. Briefly, seawater samples were added to 20 mL vials, sealed with gray butyl septa and aluminum crimp, and purged with N_2 gas for 30 min to remove background atmospheric and dissolved N_2O. Following this treatment, the sparged sodium azide/acetic acid reagent was added to convert NO_2^- to N_2O. Where $[NO_2^-] > 2\ \mu M$, the volume of seawater was subsampled in order that azide treatment of the sample NO_2^- will yield 20 nanomoles of N_2O. Where $[NO_2^-]$ was $< 2\ \mu M$, 10 mL of seawater was subsampled regardless of NO_2^- concentration in order to maximize N_2O yield, as this was the maximum sample volume that could be added to sample vials. NO_2^- isotope standards RSIL 23, 7373, and 10219 were prepared at sea by diluting 200 μM stock solutions in 3 mL of NO_2^--free seawater, then purged with N_2 gas, and reacted the same way as the samples. The product N_2O was analyzed at Stanford University on a Finnigan Delta^{PLUS} XP isotope ratio mass spectrometer. Samples and standards were analyzed in parallel, with a set of standards analyzed before and after every nine samples. Values of $\delta^{15}N_{NO2} = ({}^{15}N/{}^{14}N_{NO2} \div {}^{15}N/{}^{14}N_{reference} - 1) \times 10^3$ are reported in units of per mil (‰) versus the reference atmospheric N_2. Values of $\delta^{18}O_{NO2} = ({}^{18}O/{}^{16}O_{NO2} \div {}^{18}O/{}^{16}O_{reference} - 1) \times 10^3$, where the reference is Vienna standard mean ocean water, were also measured but not included in the current study.

N and O isotopes of NO_3^- were determined at each depth from frozen samples via the "denitrifier method" [*Sigman et al.*, 2001; *Casciotti et al.*, 2002], which involves bacterial conversion of NO_3^- and NO_2^- to N_2O. Aliquots of bacteria were added to gas-tight 20 mL vials and purged with N_2 for 3.5 h to remove the background N_2O. Following this step, the volume of seawater subsample added to the bacteria was determined to yield 10 nmol of N_2O or 20 nmol of N_2O-N. For samples containing $[NO_2^-]$ greater than 0.1 μM, addition of 10 μL sulfamic acid reagent (4% sulfamic acid in 10% HCl) per 1 mL of sample was necessary to remove NO_2^- prior to analysis [*Granger and Sigman*, 2009]. These samples were neutralized after 30 min by adding 8.5 μL of 2 M NaOH per 1 mL of sample and then injected into the prepared vials. NO_3^- isotope standards USGS 32, USGS 34, and USGS 35 were prepared from 200 μM stock solutions and run in parallel with the samples, with a set of the three standards analyzed before and after every nine samples. The product N_2O was measured via isotope ratio mass spectrometry at Stanford [*McIlvin and Casciotti*, 2011], and values of $\delta^{15}N_{NO3}$ are reported in units of permil (‰) versus the reference atmospheric N_2. $\delta^{18}O_{NO3}$ measurements were also made but not included in the current study. All isotope samples were analyzed in duplicate and are reported as the average value ± 1 standard deviation.

2.3. Model Set Up

2.3.1. Determining Concentrations of ^{15}N and ^{14}N in the Nitrate and Nitrite Pools

The first step in using the NO_3^- and NO_2^- isotope data to estimate process rates was to calculate the concentrations of ^{15}N and ^{14}N in NO_3^- and NO_2^- for each sample using isotope ratio and concentration measurements of NO_3^- and NO_2^- (Figure 2). This was done for each sample from site #1 utilizing the following equations:

$$\delta^{15}N_{sam(z)} = \left(\frac{\frac{[{}^{15}N]_{sam(z)}}{[{}^{14}N]_{sam(z)}}}{\frac{[{}^{15}N]_{ref}}{[{}^{14}N]_{ref}}} - 1 \right) \times 10^3 \quad (1)$$

$$[{}^{total}N]_{sam(z)} = [{}^{15}N]_{sam(z)} + [{}^{14}N]_{sam(z)} \quad (2)$$

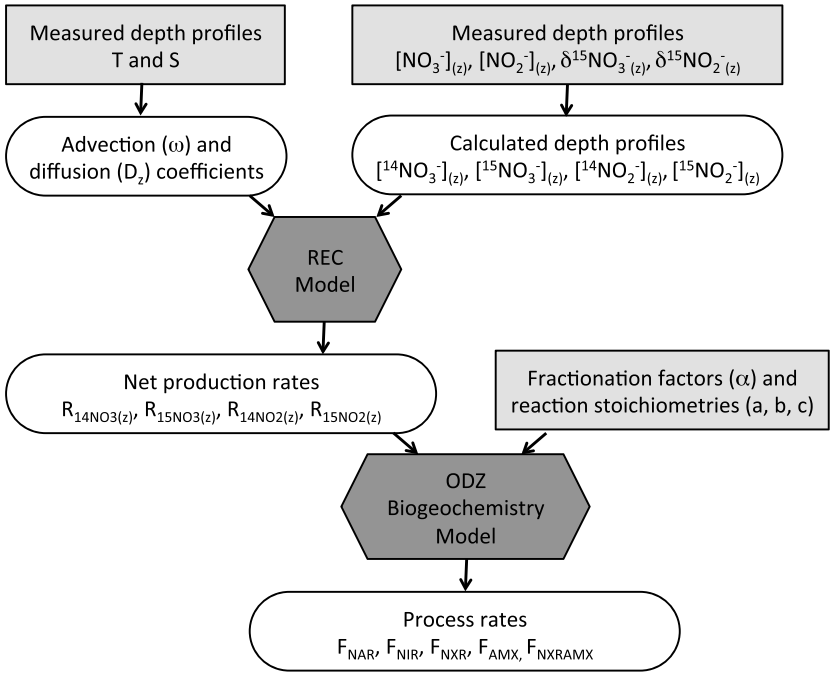

Figure 2. Flow chart of the modeling exercise.

In equation (1), $\delta^{15}N_{sam(z)}$ is the measured isotopic composition of the sample (either NO_3^- or NO_2^-) at depth z, $[^{15}N]_{sam(z)}$ and $[^{14}N]_{sam(z)}$ are the concentrations of ^{15}N and ^{14}N in the sample at z, respectively, and $[^{15}N]_{ref}/[^{14}N]_{ref}$ refers to the ratio of ^{15}N to ^{14}N in the reference, atmospheric N_2. In equation (2), $[^{total}N]_{sam(z)}$ refers to the sum of the $[^{15}N]$ and $[^{14}N]$ at a given depth, which is equal to the measured concentration of NO_3^- or NO_2^- at that depth. We can combine and rearrange equations (1) and (2) to solve for $[^{14}N]_{sam(z)}$:

$$\left[{}^{14}\mathrm{N}\right]_{\mathrm{sam}(z)} = \frac{\left[{}^{total}\mathrm{N}\right]_{\mathrm{sam}(z)}}{1 + \left(1 + \frac{\delta^{15}\mathrm{N}_{\mathrm{sam}(z)}}{10^3}\right) \times \left(\frac{\left[{}^{15}\mathrm{N}\right]_{\mathrm{ref}}}{\left[{}^{14}\mathrm{N}\right]_{\mathrm{ref}}}\right)} \tag{3}$$

We can then determine $[^{15}N]_{sam(z)}$ from equation (2). By determining $[^{14}N]$ and $[^{15}N]$ of both NO_3^- and NO_2^- at each depth, we generated four water column profiles: $[^{14}NO_2^-]_{(z)}$, $[^{15}NO_2^-]_{(z)}$, $[^{14}NO_3^-]_{(z)}$, and $[^{15}NO_3^-]_{(z)}$.

The lack of NH_4^+ accumulation is a phenomenon that has been reported previously in the ETSP ODZ, and suggests a tight coupling between ammonium production and consumption processes [*Kalvelage et al.*, 2013]. NH_4^+ concentrations determined during the pump cast were <0.1 μM within the ODZ. As isotopic analyses of NH_4^+ were not possible at these low concentrations we did not include a mass balance equation for $^{15}NH_4^+$ but instead assumed that $[^{total}NH_4^+] = [^{14}NH_4^+]$.

2.3.2. Modeling Net Rates of Nitrate, Nitrite, and Oxygen Production With the "Rate Estimation From Concentration" Model

The rate of change in concentration of a solute, C, over time can be described by the reaction-diffusion-advection equation:

$$\frac{dC}{dt} + u\frac{dC}{dx} - \frac{d}{dx}\left(D_x\frac{dC}{dx}\right) + v\frac{dC}{dy} - \frac{d}{dy}\left(D_y\frac{dC}{dy}\right) + \omega\frac{dC}{dz} - \frac{d}{dx}\left(D_z\frac{dC}{dx}\right) = R \tag{4a}$$

where u, v, and ω are the advection coefficients in the x, y, and z dimensions, respectively, D_i is the diffusion coefficient in dimension "i", and R is the net rate of production (or consumption). If the horizontal transport fluxes can be neglected (we discuss the implications of this assumption below), this equation simplifies to the following form

$$\frac{dC}{dt} + \omega\frac{dC}{dz} - \frac{d}{dx}\left(D_z\frac{dC}{dx}\right) = R \tag{4b}$$

At steady state, dC/dt becomes zero, and the net rate of production or consumption ("R") is equal to the difference between the advective and diffusive fluxes in the vertical dimension:

$$\omega \frac{dC}{dz} - \frac{d}{dz}\left(D_z \frac{dC}{dz}\right) = R \tag{4c}$$

This leads to a nonzero net rate of production (or consumption) when the difference between the advective and diffusive fluxes is nonzero.

A 1-D vertical advection-diffusion-reaction model inherently assumes that horizontal transport fluxes can be neglected and is thus necessarily a simplification of the environment in which ODZs are found. However, this assumption is justified here, especially in the upper and lower ODZ regions because the strong vertical gradients overcome weak vertical diffusivity to dominate the transport terms. Vertical gradients in NO_2^- and NO_3^- concentrations and isotopes are weaker in the middle of the ODZ, and it is possible that small horizontal transports could be important here, as discussed below. The exclusion of horizontal processes in this modeling exercise does not violate continuity because (1) the model is only run between 82 m and 350 m (that is, the model is not run all the way to the surface), and (2) a constant vertical advection term (ω) is used throughout the model.

The inverse "Rate Estimation from Concentration" ("REC") model [*Lettmann et al.*, 2012], which makes use of the simplified reactive-transport equation (4c), was used to estimate net production (or consumption) rates in the vertical dimension. The modeling exercise was conducted between 82 m and 350 m depth, which is approximately the depth range at which $[NO_2^-]$ was sufficient for isotope analysis. For the remaining discussion, the term "net production" refers to R (keeping in mind that negative net production indicates net consumption). Inputs to the REC model included $[^{14}NO_2^-]_{(z)}$, $[^{15}NO_2^-]_{(z)}$, $[^{14}NO_3^-]_{(z)}$, and $[^{15}NO_3^-]_{(z)}$ profiles from site #1, as well as vertical advection (ω) and diffusion (D_z) coefficients.

The $[^{14}NO_2^-]_{(z)}$, $[^{15}NO_2^-]_{(z)}$, $[^{14}NO_3^-]_{(z)}$, and $[^{15}NO_3^-]_{(z)}$ profiles between 82 m and 350 m depth (at 8 m resolution) were interpolated onto a computational grid to calculate rates of net production for each species ($R_{14NO2(z)}$, $R_{15NO2(z)}$, $R_{14NO3(z)}$, and $R_{15NO3(z)}$; Figure 2) at 4 m depth resolution. The second-order advection-diffusion-reaction equation (4c) was solved as a two-point boundary-value problem using Dirichlet boundary conditions, defining the value of the function (the concentration of a given chemical species) at the top (82 m) and bottom (350 m) boundaries of each profile. The Neumann boundary condition (defining the gradient of the function at the boundaries) is another option but was not pursued here. In order to incorporate the lack of NH_4^+ accumulation in the ODZ as a constraint on the model, we also made the assumption that the net production rate of NH_4^+ at each depth is equal to zero, i.e., $R_{14NH4(z)} = 0$.

We estimated vertical advection and diffusion coefficients to use in the REC model by first determining the ratio of vertical diffusion to advection (D_z/ω) at steady state with a stable conservative tracer (temperature), according to the procedure outlined by *Craig* [1969]. Since the "R" term in equation (4b) can be ignored in the case of temperature, the equation for change in temperature over time in the vertical dimension simply becomes

$$\frac{dT}{dt} = \omega \frac{dT}{dz} - \frac{d}{dz}\left(D_z \frac{dT}{dz}\right) \tag{5a}$$

At steady state, dT/dt = 0, and the vertical diffusive and advection fluxes must balance one another:

$$0 = \omega \frac{dT}{dz} - \frac{d}{dz}\left(D_z \frac{dT}{dz}\right) \tag{5b}$$

Solution of equation (5b) allows for D_z/ω to be determined from the observed temperature profile.

We then determined D_z values in the ODZ following the procedure outlined by *Osborn* [1980], *Gargett* [1984], *Gregg et al.* [1986], *Fennel and Boss* [2003], *Thorpe* [2005], and others:

$$D_z = \frac{\Gamma \varepsilon}{N^2} \tag{6a}$$

where ε is the energy dissipation rate, Γ is the mixing efficiency, and N^2 is the Brunt-Vaisala frequency. A mean $\Gamma\varepsilon$ value of 3.7×10^{-10} W kg^{-1} was estimated by *Gregg et al.* [1986] for the thermocline, which we use here. N^2 can be determined from the observed density gradient:

$$N^2 = \frac{-g}{\rho} \times \frac{d\rho}{dz} \tag{6b}$$

Table 1. Description of Physical Parameters, Stoichiometric Coefficients, and Isotope Effects Used in Model

Model Parameter[†,‡]	Description	Reported Range of Values	Standard Case Values	Reference
D_z	vertical diffusion coefficient	10^{-4} to 10^{-6} $m^2 s^{-1}$	4×10^{-5}	R. Sonnerup (personal communication, 2014), *Shaffer* [1986], and *Haskell et al.* [2015];
ω	vertical advection coefficient	-10^{-6} to -10^{-8} $m s^{-1}$	-2×10^{-7}	R. Sonnerup (personal communication, 2014), *Shaffer* [1986], *Chavez and Messie* [2009], and *Haskell et al.* [2015]
a	mol of NH_4^+ released per mol of NO_2^- reduced (NIR)	0.1 to 0.13	0.11	*Anderson* [1995] and *Koeve and Kähler* [2010]
b	mol of NH_4^+ released per mol of NO_3^- reduced (NAR)	0.06 to 0.1	0.07	*Anderson* [1995] and *Koeve and Kähler* [2010]
c	mol of NO_2^- oxidized per mol of NO_2^- reduced (AMX)	0.25 to 0.35	0.3	*Strous et al.* [1998]
α_{NAR} ($^{15}\varepsilon_{NAR}$)	fractionation factor for NO_3^- reduction	1.01 to 1.025 (10 to 25‰)	1.018 (18‰)	*Granger et al.* [2008] and *Casciotti et al.* [2013]
α_{NIR} ($^{15}\varepsilon_{NIR}$)	fractionation factor for NO_2^- reduction	1.01 to 1.025 (10 to 25‰)	1.018 (18‰)	*Bryan et al.* [1983]
α_{NXR} ($^{15}\varepsilon_{NXR}$)	fractionation factor for NO_2^- oxidation	0.988 to 0.968 (−12 to −32‰)	0.978 (−22‰)	*Casciotti* [2009] and *Casciotti et al.* [2013]
α_{AMX} ($^{15}\varepsilon_{AMX}$)	fractionation factor for anammox (NO_2^- reduction)	1.012 to 1.02 (12 to 20‰)	1.016 (16‰)	*Brunner et al.* [2013]
α_{NXRAMX} ($^{15}\varepsilon_{NXRAMX}$)	fractionation factor for NO_2^- oxidation during anammox	0.97 to 0.968 (−30 to −32‰)	0.969 (−31‰)	*Brunner et al.* [2013]

[†] $\alpha = {}^{14}k/{}^{15}k$.
[‡] $({}^{15}\varepsilon) = (\alpha - 1)x10^3$.

where ρ is the observed density and g is the gravitational acceleration constant. By determining both D_z and D_z/ω, we determined the value of ω to use in the REC model. The values obtained for D_z and ω using these methods were 4×10^{-5} $m^2 s^{-1}$ and -2×10^{-7} $m s^{-1}$ (Table 1), respectively, which are in line with previous estimates from the coastal ETSP and other upwelling zones [*Pacanowski and Philander*, 1981; *Anderson et al.*, 1982; *Codispoti and Christensen*, 1985; *Chai et al.*, 2002; *Canfield*, 2006; *Chavez and Messie*, 2009]. Nonetheless, D_z and ω values were tested for sensitivity by rerunning the REC model with modest perturbations around the obtained values.

In order to determine the potential flux of O_2 into the ODZ, the [O_2] data (dashed line in Figures 4a and 5) were also analyzed using the REC model to estimate the distribution of net O_2 consumption rates required to balance physical supply of O_2, using the standard case values for D_z and ω (4×10^{-5} $m^2 s^{-1}$ and -2×10^{-7} $m s^{-1}$, respectively; Table 1).

While we recognize that steady state is an important assumption in our modeling exercise, we argue that it is appropriate to use here since NO_3^- and NO_2^- natural abundance isotope measurements are geochemical measurements that change relatively slowly despite active biogeochemical cycling. Furthermore, the NO_3^- and NO_2^- concentration and isotope trends in our study are similar to those observed previously in relevant regions of the ETSP ODZ [*De Pol-Holz et al.*, 2009; *Casciotti et al.*, 2013; *Bourbonnais et al.*, 2015; *Hu et al.*, 2016]. Lastly, as mentioned above, pump sites #1 and #2 had similar isotope and concentration profiles, suggesting that the biogeochemical interpretations, discussed below, are somewhat representative of the coastal region.

2.3.3. Modeling the Rates of Individual Processes Using an Oxygen Deficient Zone Biogeochemistry Model

The ODZ biogeochemistry model was used to find the linear combination of process rates that best fit the net rates of production of the dissolved inorganic N species (NO_3^-, NO_2^-, and NH_4^+). Specifically, the model equations were constructed using the net production rates "R_z" of the ^{14}N and ^{15}N species of NO_2^- and NO_3^- at each depth estimated from the REC model, along with our assumption that no net production of NH_4^+ occurs.

Conceptually, NO_3^- reduction consumes NO_3^- and produces NO_2^- (F_{NAR}) while oxidizing organic matter and releasing NH_4^+ ($b \times F_{NAR}$). NO_2^- reduction via denitrification consumes NO_2^- and produces N_2 (F_{NIR}) while

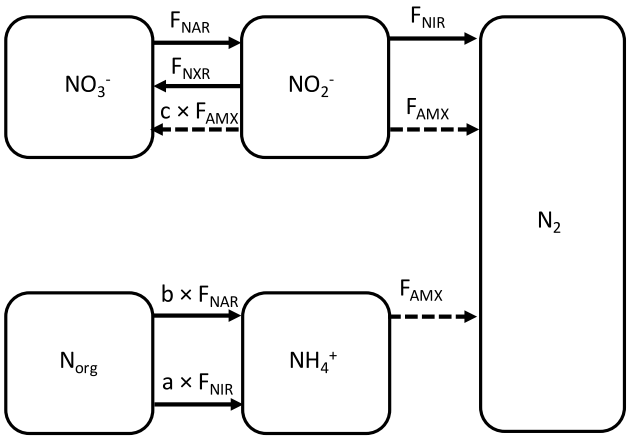

Figure 3. A schematic of the biogeochemical ODZ model describing the nitrogen cycle in marine oxygen deficient zones. The fluxes shown here are NO_3^- reduction (F_{NAR}), NO_2^- reduction (F_{NIR}), NO_2^- oxidation (F_{NXR}), and anammox (F_{AMX}). The coefficients *a* and *b* represent the moles of NH_4^+ released during NO_2^- reduction and NO_3^- reduction, respectively, while *c* refers to the moles of NO_2^- oxidized to NO_3^- per mole of NO_2^- reduced during the anammox reaction. Thus, $c \times F_{AMX}$ represents the flux of NO_2^- oxidized to NO_3^- during anammox, while F_{NXR} is the flux of NO_2^- oxidation to NO_3^- carried out by NO_2^--oxidizing bacteria.

oxidizing organic matter and releasing NH_4^+ ($a \times F_{NIR}$) (Figure 3). We assumed the organic matter has a composition described by *Anderson* [1995] and the reaction stoichiometry follows *Koeve and Kähler* [2010] such that 0.113 mol of NH_4^+ is released for every mole of NO_2^- reduced during denitrification and 0.07 mol of NH_4^+ is released for every mole of NO_3^- reduced, giving the coefficients *a* and *b*, respectively (Figure 3 and Table 1). NO_2^- oxidation consumes NO_2^- and produces NO_3^- (F_{NXR}), and anammox converts NO_2^- and NH_4^+ to N_2 in a 1:1 ratio (F_{AMX}), while oxidizing a portion of NO_2^- to NO_3^- ($F_{NXRAMX} = c \times F_{AMX}$). The amount of NO_2^- oxidized to NO_3^- during anammox has been consistently observed to occur in a ratio of 0.3 mol of NO_2^- oxidized per mole of NO_2^- reduced [*Strous et al.*, 1998; *Brunner et al.*, 2013]. Thus, the coefficient (*c*) was set to 0.3 (Table 1), and this additional flux was added to the model without adding an unknown term.

If it is assumed that the net production rates of the ^{14}N pools of NO_3^-, NO_2^-, and NH_4^+ ("$R_{14(z)}$") are made up of the fluxes associated with the ODZ biogeochemistry described above, the following equations for each model depth (*z*) can be generated:

$$R_{14NH4(z)} = a \times {}^{14}F_{NIR(z)} + b \times {}^{14}F_{NAR(z)} - {}^{14}F_{AMX(z)} \quad (7a)$$

$$R_{14NO2\,(z)} = {}^{14}F_{NAR(z)} - {}^{14}F_{AMX(z)} - c \times {}^{14}F_{AMX(z)} - {}^{14}F_{NXR(z)} - {}^{14}F_{NIR(z)} \quad (7b)$$

$$R_{14NO3(z)} = c \times {}^{14}F_{AMX(z)} + {}^{14}F_{NXR(z)} - {}^{14}F_{NAR(z)} \quad (7c)$$

where $^{14}F_{(z)}$ is the flux of ^{14}N for each N cycle process in our model defined above, calculated at depth *z*. By solving these equations at each model depth (4 m depth resolution from the REC model), the vertical distribution of these processes in the water column can be estimated.

Since rates of net production of ^{15}N-containing NO_2^- and NO_3^- were also calculated with the REC model ($R_{15(z)}$), two additional equations can be derived:

$$R_{15NO2(z)} = {}^{15}F_{NAR(z)} - {}^{15}F_{AMX(z)} - c \times {}^{15}F_{AMX(z)} - {}^{15}F_{NXR(z)} - {}^{15}F_{NIR(z)} \quad (8a)$$

$$R_{15NO3(z)} = c \times {}^{15}F_{AMX(z)} + {}^{15}F_{NXR(z)} - {}^{15}F_{NAR(z)} \quad (8b)$$

The ^{15}N fluxes can be related to the ^{14}N fluxes in the model using kinetic fractionation factors (α) (Table 1). α is related to the rate of change of [^{15}N] and [^{14}N] during a reaction by the following equation:

$$\alpha = \frac{{}^{14}F}{{}^{15}F} \times \frac{[{}^{15}N]}{[{}^{14}N]} \quad (9)$$

where ^{14}F and ^{15}F are the fluxes of ^{14}N and ^{15}N, respectively, for a particular reaction (NO_3^- reduction, NO_2^- reduction, etc.), and [^{15}N] and [^{14}N] are the concentrations of ^{15}N and ^{14}N of the substrate for the reaction [*Mariotti et al.*, 1981]. Since measurements of [^{14}N] and [^{15}N] for NO_3^- and NO_2^- were obtained at each depth, equation (9) can be rearranged to solve for ^{15}F at depth *z*:

$${}^{15}F_{(z)} = \frac{{}^{14}F_{(z)}}{\alpha} \times \frac{[{}^{15}N]_{(z)}}{[{}^{14}N]_{(z)}} \quad (10)$$

Equation (10) can then be substituted into equations (8a) and (8b), such that

$$R_{15NO2(z)} = {}^{14}F_{\frac{NAR(z)}{\alpha_{NAR}}} \times \frac{\left[{}^{15}N\,O_3^-\right]_{(z)}}{\left[{}^{14}N\,O_3^-\right]_{(z)}} - {}^{14}F_{\frac{AMX(z)}{\alpha_{AMX}}} \times \frac{\left[{}^{15}N\,O_2^-\right]_{(z)}}{\left[{}^{14}N\,O_2^-\right]_{(z)}} - c\times{}^{14}F_{\frac{AMX(z)}{\alpha_{NXRAMX}}} \times \frac{\left[{}^{15}N\,O_2^-\right]_{(z)}}{\left[{}^{14}N\,O_2^-\right]_{(z)}} - {}^{14}F_{\frac{NXR(z)}{\alpha_{NXR}}} \times \frac{\left[{}^{15}N\,O_2^-\right]_{(z)}}{\left[{}^{14}N\,O_2^-\right]_{(z)}} - {}^{14}F_{\frac{NIR(z)}{\alpha_{NIR}}} \times \frac{\left[{}^{15}N\,O_2^-\right]_{(z)}}{\left[{}^{14}N\,O_2^-\right]_{(z)}} \quad (11a)$$

$$R_{15NO3(z)} = c\times{}^{14}F_{\frac{AMX(z)}{\alpha_{NXRAMX}}} \times \frac{\left[{}^{15}N\,O_2^-\right]_{(z)}}{\left[{}^{14}N\,O_2^-\right]_{(z)}} + {}^{14}F_{\frac{NXR(z)}{\alpha_{NXR}}} \times \frac{\left[{}^{15}N\,O_2^-\right]_{(z)}}{\left[{}^{14}N\,O_2^-\right]_{(z)}} - {}^{14}F_{\frac{NAR(z)}{\alpha_{NAR}}} \times \frac{\left[{}^{15}N\,O_3^-\right]_{(z)}}{\left[{}^{14}N\,O_3^-\right]_{(z)}} \quad (11b)$$

The subscripts for each α use the same convention as their respective fluxes, with the exception of NO_2^- oxidation to NO_3^- during anammox, where α_{NXRAMX} is used to refer to the isotope fractionation that occurs during that reaction (note that this is distinct from the fractionation that occurs during the simultaneous reduction of NO_2^- to N_2 by anammox, which is denoted as "α_{AMX}").

Lastly, a system of five equations including (7a), (7b), (7c), (11a), and (11b) was used to construct a rectangular matrix to solve for the four unknown flux terms in the model at each depth ($^{14}F_{NAR(z)}$, $^{14}F_{NIR(z)}$, $^{14}F_{NXR(z)}$, and $^{14}F_{AMX(z)}$) and a residual flux that cannot be explained by the linear combination of processes described above. The nonnegative least squares (NNLS) optimization routine in MATLAB® [(called "lsqnonneg") *Lawson and Hanson*, 1974] was used to find the best fit solution, with the constraint that the fluxes must be nonnegative. We believe this is an appropriate application of NNLS, since the rates of individual N cycle processes in a real environment cannot be negative.

We note that F_{AMX} in the model was used to represent the rates of both NH_4^+ reduction and NO_2^- reduction during anammox, since NO_2^- and NH_4^+ are consumed in equal proportions to produce N_2 [*Strous et al.*, 1998]. Given that nearly all incubation measurement studies report anammox rates in terms of the N_2 produced (in units of nM N d^{-1}), those components of F_{AMX} that derive from NO_2^- and NH_4^+ were added together when reporting the modeled rates of N_2 production by anammox. This allows for a direct comparison of our modeled anammox rates with other rate measurements.

For the purposes of estimating the sensitivity of the rates of modeled biogeochemical processes to isotope effect values, the isotope effects for N cycle processes were varied within the ODZ biogeochemistry model using a Monte Carlo routine. That is, for each N cycle process, the isotope effect was varied over a range of values taken from the literature (Table 1) while holding the other isotope effects constant. The results of the sensitivity analyses are presented below.

3. Results

3.1. Observed Concentration and Isotope Profiles

O_2 concentrations (as measured by the SBE-43 dissolved O_2 sensor) at site #1 decreased rapidly from 180 μM at the surface, down to the detection limit of the instrument (~1 μM) at 95 m (Figure 4a). [O_2] remained at or below the detection limit between 95 m and 300 m and gradually increased below 300 m. STOX sensor data from previous cruises in this region [*Revsbech et al.*, 2009; *Thamdrup et al.*, 2012] and the Eastern Tropical North Pacific (ETNP) [*Tiano et al.*, 2014] suggest that [O_2] was likely lower than 10 nmol kg^{-1} (the detection limit of the STOX instrument) in the waters containing NO_2^-.

At 100 m, near the top of the ODZ, N* (defined as $[NO_3^-] + [NO_2^-] - 16 \times [PO_4^{3-}] + 2.9$ μM; modified from *Deutsch et al.* [2001]) reached a minimum value of −28 μM, characteristic for regions where N_2 is produced by denitrification and anammox (Figure 4a). The upper part of the ODZ also marks a transition between low salinity sub-Antarctic water (SAAW) and higher salinity equatorial subsurface water (ESSW) below the N* minimum (Figure 4b) [*Llanillo et al.*, 2013].

[NO_3^-] increased from 3 μM at the surface to 25 μM at 70 m (coincident with the salinity minimum) and then decreased sharply to 12 μM at 100 m (Figure 5a). The decrease in [NO_3^-] between 70 m and 100 m coincided with the bottom of the oxycline and the minimum in N* (Figure 4a). An increase in [NO_2^-] was also observed in this depth range, as [NO_2^-] rose from < 1 μM at 75 m to 3 μM at 100 m (Figure 5b). These observations

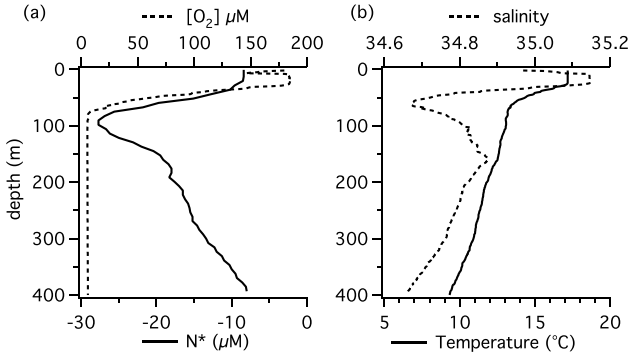

Figure 4. Vertical profiles of (a) N* (calculated as $[NO_3^- + NO_2^-] - 16\times[PO_4^{3-}] + 2.9$) (solid line) and dissolved oxygen (dashed line), and (b) temperature (solid line) and salinity (dashed line) at site #1 (20.53°S and 70.71°W). These temperature and salinity profiles were used to generate an estimate of vertical diffusion and advection.

indicate consumption of NO_3^- with production of NO_2^- and N_2 near the top of the ODZ. Between 100–150 m, $[NO_3^-]$ remained constant while $[NO_2^-]$ continued to increase, reaching a maximum of ~8 μM at 150 m. Below 150 m, $[NO_3^-]$ increased gradually to 300 m, before experiencing a sharper increase below 300 m (Figure 5a). $[NO_2^-]$ remained high (~6 to 7 μM) down to 300 m and then decreased sharply below 300 m, falling below 1 μM by 370 m (Figure 5b). The sharp decline in $[NO_2^-]$ between 300 m and 400 m occurred where $[O_2]$ began to rise at

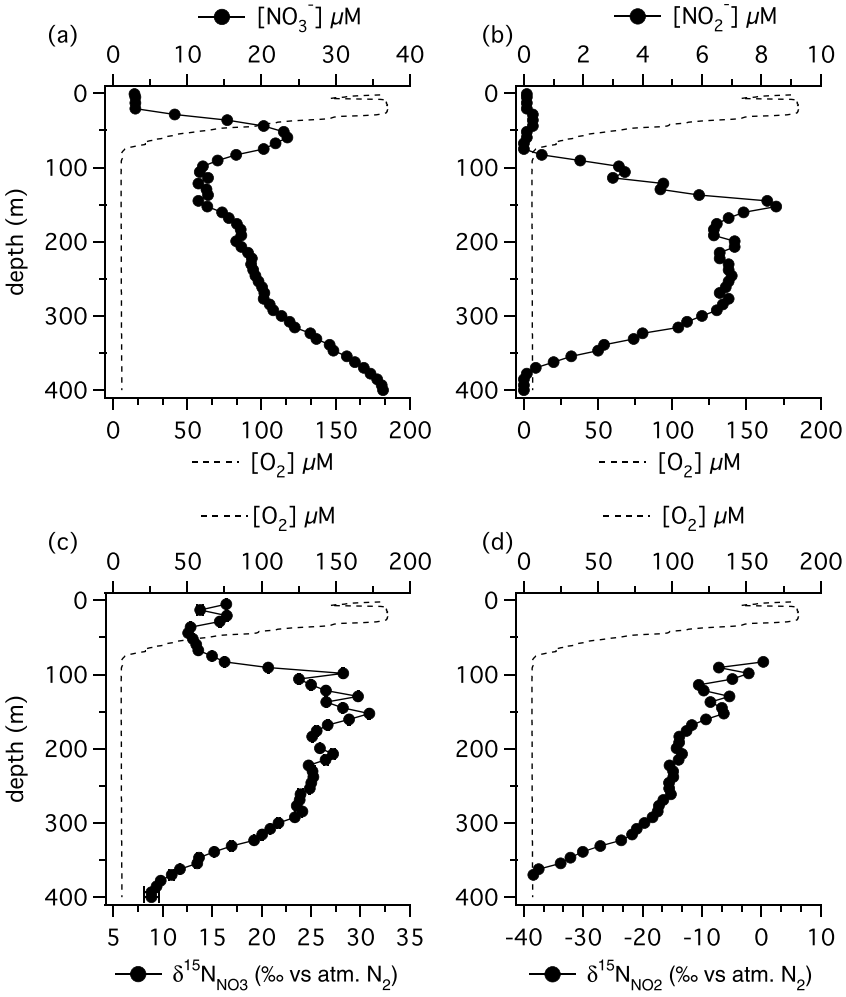

Figure 5. Concentrations of (a) NO_3^- and (b) NO_2^-, and the $\delta^{15}N$ values of (c) NO_3^- and (d) NO_2^- at pump cast site #1. Concentration and isotope measurements are indicated by closed circles, while $[O_2]$ is indicated by a dashed line. Standard deviations are included for $\delta^{15}N_{NO3}$ ($n = 2$) but not for $\delta^{15}N_{NO2}$ ($n = 1$). Note that in most cases the error bars are smaller than the data points.

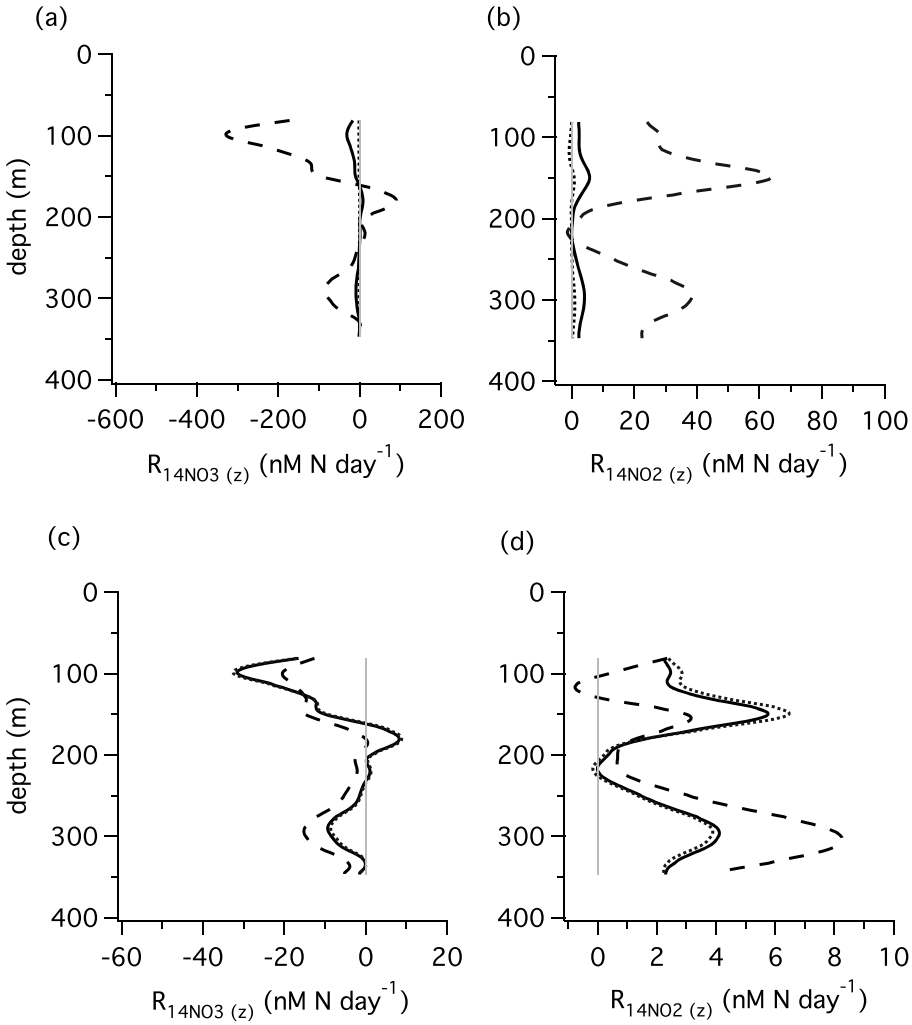

Figure 6. Net production rates of $^{14}NO_3^-$ and $^{14}NO_2^-$ at site #1 varying (a and b) diffusion coefficient (D_z) values and (c and d) advection coefficient (ω) values. The standard case, which is defined as the scenario where $D_z = 4 \times 10^{-5}$ m^2 s^{-1} and $\omega = -2 \times 10^{-7}$ m s^{-1}, is shown with a solid line in each panel. In Figures 6a and 6b the value of D_z was increased to 4×10^{-4} m^2 s^{-1} (dashed line) and decreased to 4×10^{-6} m^2 s^{-1} (dotted line) while ω was held at -2×10^{-7} m s^{-1}. In Figures 6c and 6d the value of ω was increased to -2×10^{-6} m s^{-1} (dashed line) and decreased to -2×10^{-8} m s^{-1} (dotted line) while D_z was held at $D_z = 4 \times 10^{-5}$ m^2 s^{-1}. Zero net production is indicated by the thin gray line. Note that the scales of the *x* axis are different for each panel.

the base of the ODZ (the presence of NO_2^- is likely the best indicator of functional anoxia in this study [*Thamdrup et al.*, 2012]).

$\delta^{15}N_{NO3}$ increased sharply from 15‰ at 75 m to 28‰ at 100 m (Figure 5c), coincident with the decrease in [NO_3^-] in that depth range. Below 100 m, $\delta^{15}N_{NO3}$ increased to 31‰ at 150 m and then gradually decreased in two sections, reaching 22‰ at 300 m and 9‰ at 390 m. $\delta^{15}N_{NO2}$ measurements were restricted to the depths between 82 m and 369 m, where [NO_2^-] was high enough for $\delta^{15}N_{NO2}$ analysis. $\delta^{15}N_{NO2}$ showed characteristically low values throughout the SNM, decreasing (i.e., became increasingly negative) from −7‰ at 90 m down to −38‰ at 369 m (Figure 5d). Between 100 m and 150 m, where [NO_3^-] remained constant and [NO_2^-] began to accumulate below the N* minimum, $\delta^{15}N_{NO3}$ continued to increase while $\delta^{15}N_{NO2}$ decreased. Below 150 m, $\delta^{15}N_{NO3}$ and $\delta^{15}N_{NO2}$ decreased in parallel.

Concentration and isotope profiles of NO_2^- and NO_3^- from site #2 (Figure S1) were similar to those at site #1 (Figure 5), suggesting that the observed trends in isotopes and concentrations may be regionally representative of the ETSP coastal ODZ.

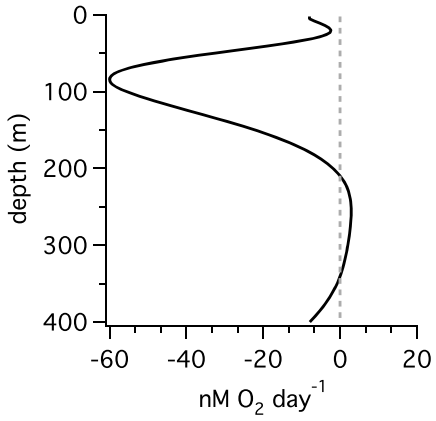

Figure 7. Profile of net production rates of O_2 from site #1 obtained with the REC model (solid line) using the standard case values for D_z (4×10^{-5} m^2 s^{-1}) and ω (-2×10^{-7} m s^{-1}). Zero production is indicated by the dotted line. Instrument error of the oxygen sensor was up to 2% of O_2 saturation, which would result in error of ± 1.7 nM O_2 d^{-1} for the net rates of O_2 production.

3.2. Rates of Net Nitrate, Nitrite, and Oxygen Production

Net consumption of NO_3^- (i.e., where $R_{14NO3(z)}$ and $R_{15NO3(z)} < 0$) was found between 82 m and ~150 m, with a maximum in consumption rate at 100 m (Figures 6a and 6c). Consumption of NO_3^- in this depth range is consistent with the sharp decrease in [NO_3^-] (Figure 5a), increase in [NO_2^-] (Figure 5b), and the minimum in N* (Figure 4a). Slight production of NO_3^- ($R_{14NO3(z)}$ and $R_{15NO3(z)} > 0$) was found between 150 m and 200 m when the highest diffusion rate ($D_z = 4 \times 10^{-4}$ m^2 s^{-1}, dashed line in Figure 6a) was used, while negligible net production was apparent with the two lower diffusion rates ($D_z = 4 \times 10^{-6}$ m^2 s^{-1}, dotted line and 4×10^{-5} m^2 s^{-1}, solid line). Net consumption of NO_3^- was predicted again, albeit at lower rates, between 250 m and 325 m where the slope of [NO_3^-] versus depth changed (Figure 5a).

Net NO_2^- production was found between 82 m and ~200 m, with a maximum at 150 m (Figures 6b and 6d), just below the maximum in NO_3^- consumption. This is also consistent with the strong gradient in [NO_2^-] observed in this depth range (Figure 5b) and the minimum in N* above it. Negligible production of $^{14}NO_2^-$ and $^{15}NO_2^-$ occurred between 200 m and 225 m ($R_{14NO2(z)}$ and $R_{15NO2(z)} \sim 0$), although net production of NO_2^- was found again between 225 m and 350 m, with a local maximum present at 300 m where a change in slope of [NO_2^-] versus depth occurred (Figure 5b).

The net rates of $^{14}NO_3^-$ and $^{14}NO_2^-$ production at each depth were sensitive to D_z values between 4×10^{-4} and 4×10^{-6} m^2 s^{-1} (Figures 6a and 6b), and less sensitive to ω variations of the same order of magnitude (Figures 6c and 6d). Variations in ω and D_z affected the magnitude of the net rates but not the sign (production versus consumption). The net rates were not sensitive to the small uncertainties in measured concentrations or isotope ratios (Figure S3). Net production of $^{15}NO_3^-$ and $^{15}NO_2^-$ showed similar patterns as the ^{14}N species but with different magnitudes related to the correspondingly lower concentrations of ^{15}N species and the isotopic fractionation factors (Figure S2).

Net consumption of O_2 occurred between 25 and 200 m, extending within the ODZ, with a maximum rate of -60 nM O_2 d^{-1} at 80 m depth (Figure 7). Slight production of O_2 was suggested by the model between 225 and 350 m (less than 5 nM O_2 d^{-1}), although this is likely an artifact, and slight consumption of O_2 was inferred between 350 and 400 m (up to -5 nM O_2 d^{-1}), where O_2 concentrations began to increase below the ODZ. Instrument error of the oxygen sensor was up to 2% of O_2 saturation, which would result in error of only ± 1.7 nM O_2 d^{-1} for the net rates of O_2 production. Uncertainty associated with D_z and ω values leads to uncertainty in the magnitude of the fluxes, but not the distribution with depth, as discussed for N transformations. So long as O_2 supply and N fluxes are estimated using the same D_z and ω values, the fluxes are directly comparable.

3.3. Modeled Rates of Individual Nitrogen Cycle Processes

Sensitivity of individual N process rates to ω and D_z was also tested (Figure S4). Like the net rates, the individual process rates from the ODZ biogeochemistry model were more sensitive to D_z than ω. Modeled rates varied by less than ~30% for variations in ω over 2 orders of magnitude. In contrast, modeled rates were negligible when $D_z = 4 \times 10^{-6}$ m^2 s^{-1} and reached unrealistically high values when $D_z = 4 \times 10^{-4}$ m^2 s^{-1} (up to 560 nM d^{-1} and 304 nM d^{-1} for NO_3^- reduction and NO_2^- oxidation, respectively; these are excluded from the figure).

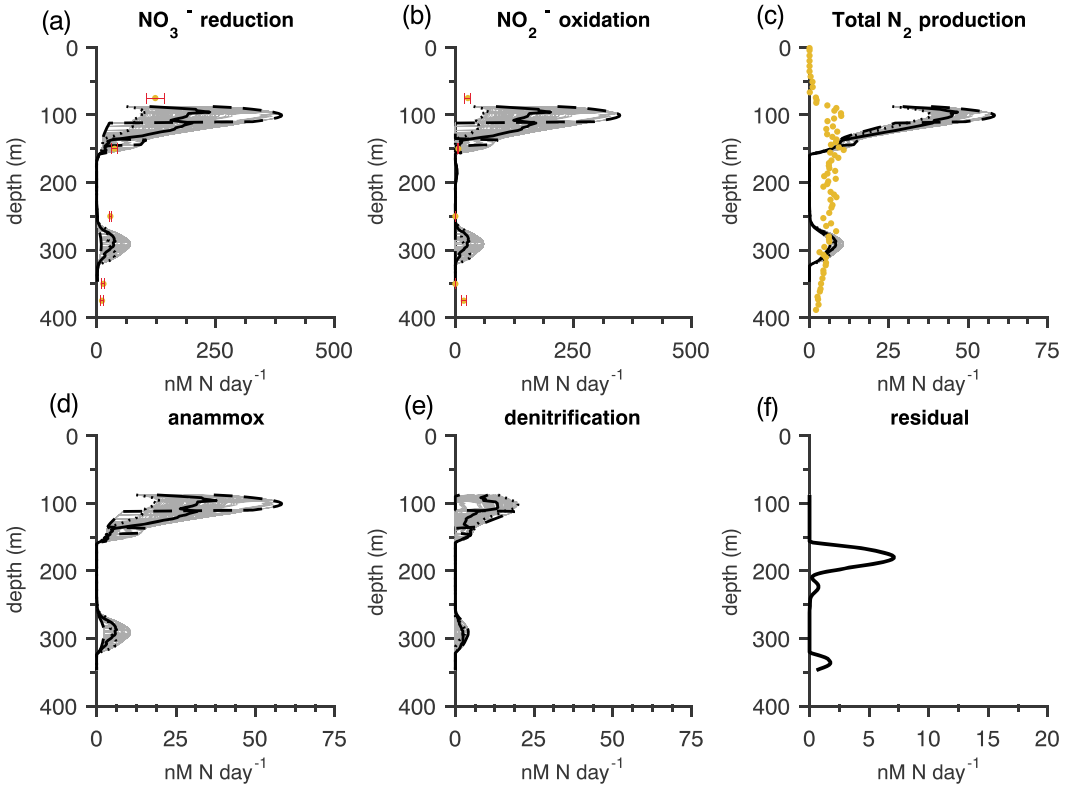

Figure 8. Sensitivity of modeled rates of (a) NO_3^- reduction, (b) NO_2^- oxidation, (c) total N_2 production, (d) anammox, and (e) denitrification to the isotope effect for NO_3^- reduction ($^{15}\varepsilon_{NAR}$), determined from a Monte Carlo simulation. Isotope effects for the other N cycle processes are held constant at intermediate values ($^{15}\varepsilon_{NXR} = -22‰$, $^{15}\varepsilon_{NIR} = 18‰$, $^{15}\varepsilon_{AMX} = 16‰$, and $^{15}\varepsilon_{NXRAMX} = -31‰$). $^{15}\varepsilon_{NAR}$ is initially set to 18‰ (solid black line, the standard case scenario) and disturbed by ± 5‰. The rates from each individual ensemble run ($n = 100$) are shown in gray. The dashed line indicates when $^{15}\varepsilon_{NAR}$ is set to 13‰ (low $^{15}\varepsilon_{NAR}$ scenario), and the dotted line denotes when $^{15}\varepsilon_{NAR}$ is set to 23‰ (high $^{15}\varepsilon_{NAR}$ scenario). (f) The sum of the residuals, which is an estimate of the error of the fit for the nonnegative least squares solution to the biogeochemical ODZ model equations. We report anammox and denitrification rates in terms of N_2 produced (in units of nM N d^{-1}), which requires that F_{AMX} be multiplied by 2. Measured rates of NO_3^- reduction, NO_2^- reduction, and N_2 production from incubation experiments by A. R. Babbin et al. (submitted, 2016) are indicated by the closed circles in Figures 8a–8c.

However, while the magnitude of modeled rates was sensitive to D_z, the shape of the rate profiles was not. For the remaining analyses the D_z and ω values obtained from the observed temperature and salinity profiles in the pump cast (4×10^{-5} m^2 s^{-1} and -2×10^{-7} m s^{-1}, respectively) were used.

In addition to sensitivity to physical parameters D_z and ω, modeled N transformation rates were sensitive to isotope effects for NO_3^- reduction and NO_2^- oxidation, with the rates of NO_3^- reduction and NO_2^- oxidation being particularly sensitive to changes in isotope effects for these processes (Figures 8 and S5). Sensitivity to isotope effects of other processes was negligible (Figures S6–S8). To test the sensitivity of process rates to variations in $^{15}\varepsilon_{NAR}$ (Figure 8), we ran the ODZ biogeochemistry model 100 times with a Monte Carlo type simulation, varying $^{15}\varepsilon_{NAR}$ around a standard value of 18‰ (solid black line), between 13‰ (dashed line) and 23‰ (dotted line) while keeping all other isotope effects at standard values (Table 1). The gray lines in Figure 8 represent results from each of the individual runs. In each case there were peaks of activity in the upper ODZ (100–150 m) and in the lower ODZ (250–325 m), with little activity in the core of the ODZ (150–250 m) (Figure 8). When $^{15}\varepsilon_{NAR} = 18‰$, NO_3^- reduction in the upper ODZ reached 225 nM N d^{-1}, with 200 nM N d^{-1} NO_2^- oxidation, 40 nM N d^{-1} anammox, and 15 nM N d^{-1} NO_2^- reduction (denitrification). When $^{15}\varepsilon_{NAR}$ was decreased to 13‰, rates of NO_3^- reduction and NO_2^- oxidation in the upper ODZ increased to ~400 nM and 350 nM N d^{-1}, respectively, while anammox rates reached ~60 nM N d^{-1}. Increasing $^{15}\varepsilon_{NAR}$ to 23‰ produced the lowest rates of NO_3^- reduction and NO_2^- oxidation in the upper ODZ (~100 nM N d^{-1}), as well as the lowest rate of anammox (20 nM N d^{-1}). This scenario did, however, yield the highest rate of denitrification (up to 20 nM N d^{-1}).

The sensitivity of the modeled rates to the isotope effect for NO_2^- oxidation ($^{15}\varepsilon_{NXR}$) was tested by varying $^{15}\varepsilon_{NXR}$ around a standard value of −22‰ between −17‰ and −27‰ (Figure S5) while holding the isotope effects for other processes at their standard case values (Table 1). Increasing $^{15}\varepsilon_{NXR}$ to −17‰ resulted in rates of NO_3^- reduction and NO_2^- oxidation that were 27% higher than the standard scenario and nearly indistinguishable from those achieved when $^{15}\varepsilon_{NAR}$ was decreased to 13‰. Decreasing $^{15}\varepsilon_{NXR}$ to −27‰ resulted in rates that were 50% lower than the standard scenario and nearly indistinguishable from those when $^{15}\varepsilon_{NAR}$ was increased to 23‰. Given that these scenarios produced similar rates to our tests of $^{15}\varepsilon_{NAR}$, we decided to group the $^{15}\varepsilon_{NXR}$ and $^{15}\varepsilon_{NAR}$ tests into three scenarios: (i) the "standard case" scenario with intermediate isotope effect values for both $^{15}\varepsilon_{NXR}$ (−22‰) and $^{15}\varepsilon_{NAR}$ (18‰), (ii) a "low $^{15}\varepsilon_{NAR}$" scenario where $^{15}\varepsilon_{NAR}$ was decreased to 13‰ or $^{15}\varepsilon_{NXR}$ was increased to −17‰, and (iii) a "high $^{15}\varepsilon_{NAR}$" scenario where $^{15}\varepsilon_{NAR}$ was increased to 23‰ or $^{15}\varepsilon_{NXR}$ was decreased to −27‰.

Residuals between 82–150 m were near zero (Figure 8f), suggesting the processes included in our model capture the primary sources and sinks of NO_3^- and NO_2^- in that region. Residuals were higher (5–10 nM N d^{-1}) in the core of the ODZ, where vertical gradients of NO_2^- and NO_3^- were weakest. One possible explanation for the high residuals in the ODZ core is simple overfitting; that is, the model struggles to find a solution when the net rates are negligible. Alternatively, while our model includes many of the key N cycle processes in the ODZ, the high residuals in the middle of the ODZ could have also resulted from excluding certain N cycle processes from the model. Residuals could also arise if horizontal transport fluxes are more important in the middle of the ODZ, although a high transport flux would likely require high horizontal velocities, as the concentration gradients in the horizontal dimensions are generally much weaker than those in the vertical dimension. Nonetheless, it is plausible that rates of N cycle processes in the ODZ core could be more accurately modeled if appropriate sampling is performed in the horizontal direction (i.e., along isopycnals), as well as the vertical dimension.

3.4. Comparison of Model Results to Rate Measurements From Incubation Experiments

Rates of NO_3^- reduction and NO_2^- oxidation were measured during the same cruise from ^{15}N incubations at a CTD cast at site #1 (A. R. Babbin et al., submitted, 2016). High-resolution rates of N_2 production were also determined from ^{15}N incubation experiments conducted from the pump cast (A. R. Babbin et al., submitted , 2016). Measured rates of NO_3^- reduction were ~125 nM N d^{-1} in the upper ODZ and decreased with depth through the ODZ (Figure 8a). These measured rates of NO_3^- reduction best fit the modeled rates of NO_3^- reduction under the high $^{15}\varepsilon_{NAR}$ scenario but were exceeded by modeled rates under the standard case and low $^{15}\varepsilon_{NAR}$ scenarios (Figure 8a). Measured rates of NO_2^- oxidation reached 20 nM N d^{-1} in the upper ODZ (Figure 8b), which was slightly lower than previous rate measurements from the ETSP ODZ (65 nM N d^{-1}) [*Kalvelage et al*., 2013]. Modeled rates of NO_2^- oxidation exceeded measured rates in all scenarios but were closest in the high $^{15}\varepsilon_{NAR}$ scenario (75 nM N d^{-1}). Modeled NO_2^- oxidation rates in the standard case and low $^{15}\varepsilon_{NAR}$ scenarios yielded even higher rates of NO_2^- oxidation in the upper ODZ (Figure 8b). Rates of N_2 production in ^{15}N incubation experiments measured using water samples collected from the same PPS deployment peaked at 18 nM N d^{-1} between 100 and 150 m (Figure 8c). Modeled rates of N_2 production again exceeded measured rates in all scenarios but were closest (46 nM N d^{-1}) in the high $^{15}\varepsilon_{NAR}$ scenario (Figure 8c).

Modeled rates of anammox showed peaks at 100 m and 280 m and reached values of 23, 38, and 62 nM N d^{-1} in the upper ODZ for the high $^{15}\varepsilon_{NAR}$, standard case, and low $^{15}\varepsilon_{NAR}$ scenarios, respectively. The modeled rates of anammox from this study were similar to the median anammox rate measured by *Kalvelage et al*. [2013] (21 nM N d^{-1}) and *De Brabandere et al*. [2014] (up to ~36 nM N d^{-1}) in the coastal ODZ of the ETSP. Rates of denitrification (NO_2^- reduction) from the ODZ biogeochemistry model reached 23 nM N d^{-1} in the upper ODZ and 7 nM N d^{-1} in the lower ODZ but showed negligible denitrification between 150 and 250 m (Figure 8e). Previous studies in this region have also found denitrification rates to be low (<20 nM N d^{-1} [*De Brabandere et al*., 2014]), or even absent [*Thamdrup et al*., 2006], although patches of higher denitrification activity have also been observed in this region of the ETSP (~30 nM N d^{-1} [*Dalsgaard et al*., 2012; *Kalvelage et al*., 2013]).

These comparisons between measured and modeled rates of NO_3^- reduction and NO_2^- oxidation suggest that $^{15}\varepsilon_{NAR}$ values of 18 to 23‰ and/or $^{15}\varepsilon_{NXR}$ values of −22 to −27‰ may be more appropriate for the ETSP ODZ than the low ε_{NAR} scenario. Furthermore, since O_2 is thought to be the primary electron acceptor required for NO_2^- oxidation, it might be expected that NO_2^- oxidation rates would be lowest in the ODZ

Table 2. Comparing the Fates of NO_2^- in the Upper and Lower ODZ and Estimation of the Relative Importance of Anammox to NO_2^- Reduction and N_2 Production From Model Results[a]

Scenario	% of NO_2^- Oxidized [b]	% of NO_2^- Reduced [c]	% of NO_2^- Lost as Anammox [d]	% of N_2 Produced by Anammox[e]
Standard Case Scenario: $^{15}\varepsilon_{NAR} = 18‰$, $^{15}\varepsilon_{NXR} = -22‰$				
Upper ODZ (90 to 150 m)	84% (6 to 91)	16% (9 to 94)	55% (23 to 91)	71% (37 to 95)
Lower ODZ (260 to 320 m)	87% (7 to 92)	13% (8 to 93)	70% (23 to 100)	82% (37 to 100)
Low $^{15}\varepsilon_{NAR}$ *Scenario*: $^{15}\varepsilon_{NAR} = 13‰$, $^{15}\varepsilon_{NXR} = -22‰$ *or* $^{15}\varepsilon_{NAR} = 18‰$, $^{15}\varepsilon_{NXR} = -17‰$				
Upper ODZ (90 to 150 m)	88% (5 to 92)	12% (7 to 95)	67% (18 to 100)	80% (31 to 100)
Lower ODZ (260 to 320 m)	7% (6 to 15)	93% (84 to 94)	24% (22 to 60)	39% (36 to 74)
High $^{15}\varepsilon_{NAR}$ *Scenario*: $^{15}\varepsilon_{NAR} = 23‰$, $^{15}\varepsilon_{NXR} = -22‰$ *or* $^{15}\varepsilon_{NAR} = 18‰$, $^{15}\varepsilon_{NXR} = -27‰$				
Upper ODZ (90 to 150 m)	72% (6 to 82)	28% (18 to 94)	36% (22 to 49)	53% (36 to 65)
Lower ODZ (260 to 320 m)	88% (77 to 92)	12% (8 to 23)	74% (45 to 100)	84% (62 to 100)

[a]Note that the percentages above are calculated using the depth-integrated rates ("*I*") of each process over the specified depth intervals (i.e., 90 to 150 m for the upper ODZ and 260 to 320 m for the lower ODZ). The values in parentheses indicate the range of each percentage at each depth sampled within those ranges.
[b]Calculated as $(I_{NXR} + c{\times}I_{AMX})/(I_{NXR} + c{\times}I_{AMX} + I_{NIR} + I_{AMX}) \times 100$
[c]Calculated as $(I_{NIR} + I_{AMX})/(I_{NXR} + c{\times}I_{AMX} + I_{NIR} + I_{AMX}) \times 100$
[d]Calculated as $(I_{AMX})/(I_{NIR} + I_{AMX}) \times 100$
[e]Calculated as $(2{\times}I_{AMX})/(I_{NIR} + 2{\times}I_{AMX}) \times 100$

core, where O_2 concentrations and supply rates are likely to be lowest. Both the measurements and model results suggest that this is the case.

3.5. Examining the Fate of Nitrite in Oxygen Deficient Zones

One of the primary goals of this study was to assess the fate of NO_2^- produced in the ODZ. Specifically, we aimed to determine how much NO_2^- was being lost, via NO_2^- reduction to N_2 by anammox (F_{AMX}) and denitrification (F_{NIR}), versus how much NO_2^- was being retained, via oxidation back to NO_3^- by NO_2^- oxidation (F_{NXR}) and anammox (F_{NXRAMX}). In order to accomplish this, the depth-integrated rates of each process (I_X, where "X" indicates a specific process) were calculated across the upper ODZ (90 to 150 m) and across the lower ODZ (260 to 320 m). For each zone, the percentage of reacted NO_2^- that was lost by reduction was determined using the depth-integrated rates:

$$\frac{I_{NIR} + I_{AMX}}{I_{NXR} + c{\times}I_{AMX} + I_{NIR} + I_{AMX}} \times 100 \tag{12a}$$

A similar calculation was also performed to determine the percentage of NO_2^- that was oxidized back to NO_3^-, representing the retention of fixed N:

$$\frac{I_{NXR} + c{\times}I_{AMX}}{I_{NXR} + c{\times}I_{AMX} + I_{NIR} + I_{AMX}} \times 100 \tag{12b}$$

All scenarios resulted in high percentages of NO_2^- retention in the upper ODZ (72–88%; Table 2). In the lower ODZ, the standard case scenario and high $^{15}\varepsilon_{NAR}$ scenario resulted in high fractions of NO_2^- retention (87% and 88%, respectively), while only 7% of NO_2^- was retained under low $^{15}\varepsilon_{NAR}$ scenario.

In addition to estimating the oxidative and reductive fates of NO_2^- in the ODZ, our study aimed to better understand the fractional contributions of anammox to NO_2^- removal and N_2 production. Using the depth-integrated rates in the upper ODZ and lower ODZ, the following calculations were performed to estimate the percentage of reduced NO_2^- that is consumed by anammox and the relative contribution of anammox to N_2 production, respectively:

$$\frac{I_{AMX}}{I_{NIR} + I_{AMX}} \times 100 \tag{13a}$$

$$\frac{2{\times}I_{AMX}}{I_{NIR} + 2{\times}I_{AMX}} \times 100 \tag{13b}$$

Note that in equation (13b) the F_{AMX} rates are multiplied by 2 to yield an estimate of the total dissolved inorganic nitrogen ($NO_2^- + NH_4^+$) converted to N_2 by anammox. Here there was more of a distinction between the standard case scenario and high $^{15}\varepsilon_{NAR}$ scenario (Table 2). In the standard case scenario, anammox made

up 55% of NO_2^- reduced to N_2 in the upper ODZ, and 70% in the lower ODZ, while the high $^{15}\varepsilon_{NAR}$ scenario resulted in 36% NO_2^- reduction via anammox in the upper ODZ, and 74% in the lower ODZ. In the low $^{15}\varepsilon_{NAR}$ scenario, 67% and 24% of the NO_2^- reduced was due to anammox in the upper and lower ODZ, respectively.

Since only one of the N atoms in the N_2 produced by anammox is derived from NO_2^- (with the other N atom coming from NH_4^+), the fraction of N_2 production due to anammox is necessarily greater than the fraction of NO_2^- removal reduction due to anammox (Table 2). Under the standard case scenario, anammox was responsible for 71% of N_2 production in the upper ODZ and 82% of N_2 production in the lower ODZ. Similarly, in the high $^{15}\varepsilon_{NAR}$ scenario anammox contributed 53% and 84% to N_2 production in the upper and lower ODZ, respectively. The low $^{15}\varepsilon_{NAR}$ scenario resulted in anammox contributions of 80% in the upper ODZ and 39% in the lower ODZ.

Evaluating whether transport of O_2 into the ODZ could support the inferred rates of NO_2^- oxidation, the integrated net rate of O_2 production in the upper ODZ over the interval 90 to 150 m was -2.7 mmol O_2 m^{-2} d^{-1}. Since 1 mol of O_2 can support 2 mol of NO_2^- oxidation to NO_3^-, this value was multiplied by 2 to obtain an estimated NO_2^- oxidation rate of 5.4 mmol N m^{-2} d^{-1} that could be supported by O_2 supply in the upper ODZ. This supported rate of NO_2^- oxidation exceeds the integrated NO_2^- oxidation rates over the same depth interval under the high $^{15}\varepsilon_{NAR}$ scenario (2.9 mmol N m^{-2} d^{-1}) and is close to the rate of NO_2^- oxidation in the standard case scenario (6.4 mmol N m^{-2} d^{-1}). On the other hand, the O_2 flux would not support the inferred rate of NO_2^- oxidation in the low $^{15}\varepsilon_{NAR}$ scenario (8.6 mmol N m^{-2} d^{-1}). For the lower ODZ, the integrated O_2 production rate was 0.1 mmol O_2 m^{-2} d^{-1} over the depth range 260 m to 320 m, resulting from the much smaller gradient in O_2 concentration in the lower ODZ. This O_2 flux from below would not support the integrated rates of NO_2^- oxidation from the model over the same depth interval under any of the model scenarios tested (ranging from negligible NO_2^- oxidation rates under the low $^{15}\varepsilon_{NAR}$ scenario to 1.7 mmol N m^{-2} d^{-1} in the high $^{15}\varepsilon_{NAR}$ scenario).

4. Discussion

4.1. Comparison Between Measured and Modeled Rates of N Cycle Processes

The N isotope measurements represent an integrated record of N cycle processes that have occurred in a given water parcel, and the model results represent a time-averaged estimate of process rates. Therefore, the presence of a particular N cycle process (such as NO_2^- oxidation) in our model output does not necessarily imply that the process was occurring at our study site at the time of sampling or that the process was occurring across the ETSP ODZ as a whole. If the process occurs sporadically, the natural abundance isotopes will smooth that spatial or temporal variability to a steady average rate. In contrast, the incubation-based rate measurements reflect the rate of a given N cycle process at the time of sampling and may show higher or lower rates than estimated from our model. The different temporal and spatial scales of the isotope measurements and rate measurements make these two approaches complementary. In particular, the opposing isotope effects for NO_2^- oxidation and NO_2^- reduction, together with the requirement for complete NH_4^+ consumption, set strong constraints on the rates of N cycling in our ODZ biogeochemistry model.

Our model predicts secondary maxima in rates of most processes at the bottom of the ODZ. This derives directly from the NO_3^- and NO_2^- concentration profiles and net production estimates (Figure 6), which show NO_3^- consumption and NO_2^- production in the lower ODZ. Measured NO_2^- oxidation rates also reached a secondary peak at the bottom of the ODZ, though much lower than the upper peak. Vertical transport of O_2 was evaluated using the REC model but was found to be insufficient to support the modeled rates of NO_2^- oxidation in the lower ODZ. The peaks in denitrification and NO_3^- reduction at the bottom of the ODZ are also difficult to explain given the dependence of these processes on organic matter supply [*Kalvelage et al*., 2013; *Ward*, 2013; *Babbin et al*., 2014]. While profiles of [NO_3^-] and [PO_4^{3-}] suggest that more remineralization might have occurred in the lower ODZ than the middle ODZ (Figure S9), we suspect the denitrification peak in the lower ODZ may also be due to horizontal transport of water from regions of more intense N removal, such as waters closer to the continental shelf.

The similarity in NO_2^- and NO_3^- concentrations and isotope distributions between sites #1 and #2 suggests that the observed trends are, to some degree, representative of the region. However, a mismatch between previously measured rates of denitrification and the modeled rates in this study could arise from limitations caused by the one-dimensional formulation of the model. Namely, the negligible rates in the middle of the

ODZ could be a consequence of the model assumption that the horizontal transports are zero. Horizontal transport of upwelled waters has been documented in this coastal upwelling region [*Chavez and Messie*, 2009; *Pietri et al*., 2013]. If the denitrification signal manifests itself as a horizontal change in concentration or $\delta^{15}N$ in this zone, this would be missed in the 1-D analysis.

4.2. Comparison to Other Model Studies

An early 1-D advection-diffusion-reaction model study of N cycling in ODZs suggested that NO_2^- produced in the ETSP ODZ was consumed by reduction and oxidation in roughly equal parts [*Anderson et al*., 1982]. *Casciotti et al*. [2013] tested this hypothesis by incorporating N isotope measurements from the ETSP ODZ into a one-dimensional isopycnal model and found that this partitioning between NO_2^- oxidation and NO_2^- reduction could be replicated when $^{15}\varepsilon_{NAR} = 10‰$ and $^{15}\varepsilon_{NXR} = -32‰$. In that scenario, roughly similar fractions of fixed N retention (50% in the upper ODZ and 80% in the lower ODZ) and loss occurred within the ODZ [*Casciotti et al*., 2013].

In our model, the fraction of NO_2^- retention in the upper ODZ was even higher (72% to 88%) under all scenarios tested, including the isotope effects used by *Casciotti et al*. [2013], which gave results similar to our standard case model (not shown). In this study, estimates of fixed N retention were similar to those from *Casciotti et al*. [2013] in the lower ODZ when applying the standard case and high $^{15}\varepsilon_{NAR}$ scenarios. In contrast, the patterns of NO_2^- oxidation and reduction observed in low $^{15}\varepsilon_{NAR}$ scenario were inconsistent with a variety of studies measuring the distribution of these processes in instantaneous rate measurements and yielded unrealistically high rates of NO_3^- reduction. In discounting that scenario, our study suggests a best fit to available data using $^{15}\varepsilon_{NXR}$ values lower (more negative) than −17‰, consistent with *Casciotti et al*. [2013] and a relatively high fraction of NO_2^- reoxidized.

A recent study by *Buchwald et al*. [2015] constrained rates of N cycle processes in the ETNP ODZ using N and O isotope measurements in a 1-D vertical reaction-diffusion-advection forward model and found that approximately equal rates of NO_2^- oxidation and NO_2^- reduction were needed to fit the NO_3^- and NO_2^- isotope data. While that model prescribed initial concentrations and isotopic compositions of NO_3^- and NO_2^-, and parameterized the rate constants for N processes, our approach did not require these assumptions but yielded similar results. Thus, we believe this study represents an advance over previous work by reducing the number of assumptions and parameters used to tune the model. Finally, previous studies did not attempt to separate NO_2^- oxidation and reduction due to anammox from those due to NO_2^- oxidizing bacteria and denitrifying bacteria, respectively.

In doing so, the modeling exercise in this study has revealed some interesting trends. For example, our model suggests that the recycling of NO_2^- back to NO_3^- is largely due to NO_2^- oxidation (F_{NXR}) rather than anammox (F_{NXRAMX}), as the rates of NO_2^- oxidation are generally much greater than those of anammox. Specifically, F_{NXRAMX} was only responsible for ~6% of the total NO_2^- oxidized in the upper ODZ, while NXR made up 94% of the total NO_2^- oxidized. Thus, anammox seems to be responsible for only a small percentage of the total NO_2^- oxidized in the ODZ. This may be surprising since $[O_2]$ is very low in the ODZ and is thought to be necessary for NO_2^- oxidation. However, results from the REC model suggest that the integrated O_2 consumption rates in the upper ODZ could support the NO_2^- oxidation rates under the high $^{15}\varepsilon_{NAR}$ scenario and nearly support those in the standard case scenario, but not the low $^{15}\varepsilon_{NAR}$ scenario. We argue above that the low $^{15}\varepsilon_{NAR}$ scenario is unlikely to be correct and further note that alternate electron acceptors would be required to oxidize NO_2^- in the absence of a sufficient O_2 flux in this scenario. The close match in distribution and absolute rates of NO_3^- reduction and NO_2^- oxidation suggests that these processes are tightly coupled and lend some support to the hypothesis of *Kemeny et al*. [2016] that NO_2^- oxidizing bacteria might catalyze the interconversion of NO_3^- and NO_2^- under conditions unfavorable for their growth. We cannot determine the exact mechanism for NO_2^- oxidation in the ODZ from the model results in this study, but we do believe this warrants further examination.

4.3. Anammox Versus Denitrification, Revisited

Given the average stoichiometry of marine organic matter, theoretical predictions and field data suggest that anammox should be responsible for ~28% of the total N_2 produced during fixed N loss [*Strous et al*., 1998; *Koeve and Kähler*, 2010; *Dalsgaard et al*., 2012; *Ward*, 2013; *Babbin et al*., 2014]. This assumes that respiration of organic matter is tied stoichiometrically to heterotrophic NO_3^- and NO_2^- reduction with no accumulation

of NH_4^+ or NO_2^-. Because NO_3^- reduction produces NO_2^- and NH_4^+ in a higher proportion than that required by anammox, NO_2^- removal by denitrification is assumed to consume the NO_2^- not utilized by anammox. If an alternative NO_2^- removal pathway decouples heterotrophic NO_3^- reduction and NO_2^- reduction, the contribution of anammox to N_2 production could be higher than 28%. In other words, denitrification would not be required to consume NO_2^-, and NH_4^+ could continue to be supplied by NO_3^- reduction without accumulating excessive amounts of NO_2^-.

In our model results, the highest contributions of NO_2^- reduction by anammox generally occurred in scenarios with the highest % NO_2^- oxidized. For example, the model scenarios that came closest to the expected 28% anammox contribution to N_2 production were the high $^{15}\varepsilon_{NAR}$ scenario in the upper ODZ (53%) and the low $^{15}\varepsilon_{NAR}$ scenario in the lower ODZ (39%), which also had the lowest amount of NO_2^- oxidation. The standard case scenario had 71% and 82% of N_2 production fueled by anammox in the upper and lower ODZ (Table 2), and correspondingly higher amounts of NO_2^- oxidation (84% and 87% in the upper and lower ODZ). These high anammox % are also reflective of the instantaneously measured rates from the cruise (A. R. Babbin et al., submitted, 2016).

Although the fraction of N_2 produced by anammox was generally higher than that from denitrification, the contribution from denitrification was higher in the upper ODZ than the lower ODZ. This trend may be explained by the vertical changes in the supply of organic matter in the water column. Near the top of the ODZ, the organic supply is likely to be the highest, thus fueling processes such as heterotrophic NO_3^- and NO_2^- reduction ("denitrification"). The organic matter supply steadily decays with depth as it is consumed [*Martin et al*., 1987; *Van Mooy et al*., 2002; *Babbin et al*., 2014], and thus heterotrophic processes should be less prominent deeper in the ODZ. Anammox, on the other hand, is an autotrophic process and could play a greater role in N loss toward the bottom of the ODZ. In this case, nonheterotrophic processes would need to supply NH_4^+ for anammox. This is consistent with the findings of A. R. Babbin et al. (submitted, 2016) that suggest that the observed rates of heterotrophic NO_3^- and NO_2^- reduction cannot support the observed rates of anammox below 200 m. Some have proposed that zooplankton excretion, not included in our model, may be an important source of NH_4^+ toward the bottom of the ODZ [*Bianchi et al*., 2014].

One approach for further delineating processes in the ODZ is through the use of O isotopes in NO_3^- and NO_2^-. Even without applying the O isotope measurements, the number of tracers was sufficient to constrain the desired fluxes in the inverse model used here. However, use of O isotopes may allow inclusion of additional processes or removal of uncertainties related to N isotope effects. Future studies that aim to identify O isotope effects for anammox could strengthen the use of $\delta^{18}O$ measurements in similar analyses, thus providing tighter constraints on modeled N cycle fluxes and/or allow for additional fluxes to be modeled.

5. Conclusions

We found that high-resolution vertical sampling of natural abundance isotopes was helpful for constraining the rates of N cycle processes where vertical gradients were steep, and the highest rates of processes are likely to occur, although high-resolution vertical sampling did not necessarily improve our understanding of N cycle process in the middle of the ODZ, where the vertical gradients were weaker.

The modeled rates, as well as the fractions of fixed N retained versus fixed N lost, were sensitive to assumptions about the vertical diffusivity and isotope effects for individual processes, highlighting the need for tighter constraints on these parameters. Of the three scenarios in our modeling exercise, the high $^{15}\varepsilon_{NAR}$ scenario seemed to agree best with previously measured rates from the ETSP, suggesting that $^{15}\varepsilon_{NAR}$ values 18‰ to 23‰ and/or $^{15}\varepsilon_{NXR}$ values of −27‰ to −22‰ are most appropriate for our study site.

Modeled rates of N cycle processes suggested that NO_2^- oxidation is tightly coupled to NO_3^- reduction in the upper and lower ODZ. This allows reduced NO_3^- to be retained in the system, rather than being reduced to N_2. Moreover, while the model results yielded a large range in the relative contributions of anammox and denitrification to NO_2^- loss and N_2 production, it seems that both processes are likely to be important over the time scales at which NO_3^- and NO_2^- isotope measurements are integrated. Moreover, NO_2^- oxidation played an important role in allowing anammox and denitrification to become decoupled from the expected proportions driven by organic matter stoichiometry and could explain a higher proportion of N_2 production

from anammox versus denitrification. Considering that most global ocean models incorporating N cycle processes do not include a NO_2^- reoxidation pathway, our model results indicate that global marine N budgets might need to be revisited.

Acknowledgments
We greatly thank chief scientists Alan Devol and Bess Ward for the opportunity to participate in the ETSP 2013 cruise, as well as the captain and crew of the R/V *Nathaniel B. Palmer* for their assistance. We also thank Gadiel Alarcón for his help with the pump cast, Bonnie Chang for her help with the pump cast and helpful discussions on the biogeochemical model, and Rolf Sonnerup for his help in confirming ω and D_z estimates from the T and S profiles. This work was supported by NSF grants OCE 1140404 to K.L.C. and OCE 1233425 to C.W.M. This publication is partially funded by the Joint Institute for the Study of the Atmosphere and Ocean (JISAO) under NOAA Cooperative Agreement NA10OAR4320148 and is contribution 2436 to JISAO and contribution 4338 to NOAA's Pacific Marine Environmental Laboratory. O.U. is supported by the Millennium Scientific Initiative (grant IC 120019) and the Chilean National Commission for Scientific and Technological Research, CONICYT (grant Fondecyt 1130784). These data are publicly available by accessing the Stanford Digital Repository (http://purl.stanford.edu/bc662wj4121).

References

Anderson, J. J., A. Okubo, A. S. Robbins, and F. A. Richards (1982), A model for nitrite and nitrate isotope distributions in oceanic oxygen minimum zones, *Deep-Sea Res.*, *29*, 1113–1140, doi:10.1016/0198-0149/82/90031-0.

Anderson, L. A. (1995), On the hydrogen and oxygen content of marine phytoplankton, *Deep-Sea Res.*, *42*, 1675–1680, doi:10.1016/0967-0637(95)00072E.

Armstrong, F. A. J., C. R. Stearns, and J. D. H. Strickland (1967), The measurement of upwelling and subsequent biological processes by means of the Technicon™ AutoAnalyzer™ and associated equipment, *Deep-Sea Res.*, *14*, 381–389.

Babbin, A. R., R. G. Keil, A. H. Devol, and B. B. Ward (2014), Organic matter stoichiometry, flux, and oxygen control nitrogen loss in the ocean, *Science*, *344*, 406–408, doi:10.1126/science.1248364.

Banyte, D., T. Tanhua, M. Visbeck, D. Wallace, J. Karstensen, G. Krahmann, L. Stramma, and M. Dengler (2012), Diapycnal diffusivity at the upper boundary of the tropical North Atlantic oxygen minimum zone, *J. Geophys. Res.*, *117*, C09016, doi:10.1029/2011JC007762.

Barber, R., and F. Chavez (1983), Biological consequences of El Niño, *Science*, *222*, 1203–1210, doi:10.1126/science.222.4629.1203.

Bianchi, D., A. R. Babbin, and E. Galbraith (2014), Enhancement of anammox by the excretion of diel vertical migrators, *Proc. Natl. Acad. Sci. U.S.A.*, *111*, 15,604–15,605.

Bourbonnais, A., M. A. Altabet, C. N. Charoenpong, J. Larkum, H. Hu, H. Bange, and L. Stramma (2015), N-loss isotope effects in the Peru oxygen minimum zone studied using a mesoscale eddy as a natural tracer experiment, *Global Biogeochem. Cycles*, *29*, 793–811, doi:10.1002/2014GB005001.

Boynton, W. R., W. M. Kemp, and C. W. Keefe (1982), A comparative analysis of nutrients and other factors influencing estuarine phytoplankton production, in *Estuarine Comparisons*, edited by V. S. Kennedy, pp. 69–90, Academic Press, New York.

Brandes, J. A., A. H. Devol, T. Yoshinari, D. A. Jayakumar, and A. S. Naqvi (1998), Isotopic composition of nitrate in the central Arabian Sea and Eastern Tropical North Pacific: A tracer for mixing and nitrogen cycles, *Limnol. Oceanogr.*, *43*, 1680–1689, doi:10.4319/lo.1998.43.7.1680.

Brandhorst, W. (1959), Nitrification and denitrification in the Eastern Tropical North Pacific, *J. Conseil. Int. Explor. Mer*, *25*, 3–20.

Brunner, B., et al. (2013), Nitrogen isotope effects induced by anammox bacteria, *Proc. Natl. Acad. Sci. U.S.A.*, *110*, 18,994–18,999, doi:10.1073/pnas.1310488110.

Bryan, B. A., G. Shearer, J. Skeeters, and D. H. Kohl (1983), Variable expression of the nitrogen isotope effect associated with denitrification of nitrite, *J. Biol. Chem.*, *258*, 8613–8617.

Buchwald, C., A. E. Santoro, R. H. R. Stanley, and A. K. L. Casciotti (2015), Nitrogen cycling in the secondary nitrite maximum of the Eastern Tropical North Pacific off Costa Rica, *Global Biogeochem. Cycles*, *29*, 2061–2081, doi:10.1002/2015GB005187.

Canfield, D. E. (2006), Models of oxic respiration, denitrification, and sulfate reduction in zones of coastal upwelling, *Geochim. Cosmochim. Acta*, *70*, 5753–5765, doi:10.1016/j.gca.2006.07.023.

Casciotti, K. L. (2009), Inverse kinetic isotope fractionation during bacterial nitrite oxidation, *Geochim. Cosmochim. Acta*, *73*, 2061–2076, doi:10.1016/j.gca.2008.12.022.

Casciotti, K. L., D. M. Sigman, M. G. Hastings, J. K. Bohlke, and A. Hilkert (2002), Measurements of the oxygen isotopic composition of nitrate in seawater and freshwater using the denitrifier method, *Anal. Chem.*, *74*, 4905–4912, doi:10.1021/ac020113w.

Casciotti, K. L., C. Buchwald, and M. Mcilvin (2013), Implications of nitrate and nitrite isotope measurements for the mechanisms of nitrogen cycling in the Peru oxygen deficient zone, *Deep Sea Res., Part I*, *80*, 78–93, doi:10.1016/j.dsr.2013.05.017.

Chai, F., R. C. Dugdale, T. H. Peng, F. P. Wilkerson, and R. T. Barber (2002), One-dimension ecosystem model of the equatorial Pacific upwelling system, Part I: Model development and silicon and nitrogen cycle, *Deep Sea Res., Part II*, *49*, 2713–2745, doi:10.1016/S0967-0645(02)00055-3.

Chavez, F., and M. Messie (2009), A comparison of Eastern Boundary Upwelling Ecosystems, *Prog. Oceanogr.*, *83*, 80–96, doi:10.1016/j.pocean.2009.07.032.

Cline, R. D., and F. A. Richards (1972), Oxygen deficient conditions and nitrate reduction in the eastern tropical ocean, *Limnol. Oceanogr.*, *17*, 885–900, doi:10.4319/lo.1972.17.6.0885.

Codispoti, L. A. (1989), Phosphorus vs. nitrogen limitation of new and export production, in *Productivity of the Ocean: Present and Past*, edited by W. H. Berger et al., pp. 377–394, John Wiley, Hoboken, N. J.

Codispoti, L. A., and A. J. Christensen (1985), Nitrification, denitrification, and nitrous oxide cycling in the eastern tropical South Pacific Ocean, *Mar. Chem.*, *16*, 277–300, doi:10.1016/0304-4203(85)90051-9.

Codispoti, L. A., and F. A. Richards (1976), An analysis of the horizontal regime of denitrification in the eastern tropical North Pacific, *Limnol. Oceanogr.*, *21*, 379–388, doi:10.4319/lo.1976.21.3.0379.

Craig, H. (1969), Abyssal carbon and radiocarbon in the Pacific, *J. Geophys. Res.*, *74*, 5491–5506, doi:10.1029/JC074i023p05491.

Czeschel, R., L. Stramma, F. Schwarzkopf, B. Giese, A. Funk, and J. Karstensen (2011), Middepth circulation of the eastern tropical South Pacific and its link to the oxygen minimum zone, *J. Geophys. Res.*, *116*, C01015, doi:10.1029/2010JC006565.

Dalsgaard, T., D. E. Canfield, J. Petersen, B. Thamdrup, and J. Acuna-Gonzalez (2003), N_2 production by the anammox reaction in the anoxic water column of Golfo Dulce, Costa Rica, *Nature*, *422*, 2–4, doi:10.1038/nature01526.

Dalsgaard, T., B. Thamdrup, L. Farias, and N. P. Revsbech (2012), Anammox and denitrification in the oxygen minimum zone of the eastern South Pacific, *Limnol. Oceanogr.*, *57*, 1331–1346, doi:10.4319/lo.2012.57.5.1331.

Dalsgaard, T., F. J. Stewart, B. Thamdrup, L. D. E. Brabandere, N. P. Revsbech, O. Ulloa, D. E. Canfield, and E. F. Delong (2014), Oxygen at nanomolar levels reversibly suppresses process rates and gene expression in anammox and denitrification in the oxygen minimum zone off Northern Chile mBio, *5*, e01966-14.

De Brabandere, L., B. Thamdrup, N. P. Revsbech, and R. Foadi (2012), A critical assessment of the occurrence and extend of oxygen contamination during anaerobic incubations utilizing commercially available vials, *J. Microbiol. Methods*, *88*, 147–154.

De Brabandere, L., D. E. Canfield, T. Dalsgaard, G. E. Friedrich, N. P. Revsbech, O. Ulloa, and B. Thamdrup (2014), Vertical partitioning of nitrogen-loss processes across the oxic-anoxic interface of an oceanic oxygen minimum zone, *Environ. Microbiol.*, *16*, 3041–3054, doi:10.1111/1462-2920.12255.

De Pol-Holz, R., R. Robinson, D. Hebbeln, D. M. Sigman, and O. Ulloa (2009), Controls on sedimentary nitrogen isotopes along the Chile margin, *Deep-Sea Res.*, *56*, 1042–1054, doi:10.1016/j.dsr2.2008.09.014.

Deutsch, C., N. Gruber, R. M. Key, and J. L. Sarmiento (2001), Denitrification and N_2 fixation in the Pacific Ocean, *Global Biogeochem. Cycles*, *15*, 483–506, doi:10.1029/2000GB001291.
Deutsch, C., et al. (2014), Centennial changes in North Pacific anoxia linked to tropical trade winds, *Science*, *345*, 665–668, doi:10.1126/science.1252332.
Environmental Protection Agency (1984), Nitrogen ammonia (colorimetric, automated phenate), Method 350.1, in *Methods for Chemical Analysis of Water and Wastes*, *EPA-600/4-020*, pp. 1–14, U.S. Environmental Protection Agency, Office of Research and Development, Washington, D. C.
Escribano, R., et al. (2004), Biological and chemical consequences of the 1997–1998 El Niño in the Chilean coastal upwelling system: A synthesis, *Deep Sea Res., Part II*, *51*, 2389–2411, doi:10.1016/j.dsr2.2004.08.011.
Fennel, K., and E. Boss (2003), Subsurface maxima of phytoplankton and chlorophyll: Steady-state solutions from a simple model, *Limnol. Oceanogr.*, *48*, 1521–1534.
Fussel, J., P. Lam, G. Lavik, M. M. Jensen, M. Holtapels, and M. M. Kuypers (2012), Nitrite oxidation in the Namibian oxygen minimum zone, *ISME J.*, *6*, 1200–1209, doi:10.10138/ismej.2011.178.
Gargett, A. E. (1984), Vertical eddy diffusivity in the ocean interior, *J. Mar. Res.*, *42*, 359–393.
Goering, J. J. (1968), Denitrification in the oxygen minimum layer of the eastern tropical Pacific Ocean, *Deep-Sea Res.*, *15*, 157–164, doi:10.1016/0011-7471(68)90037-5.
Gordon, L. I., J. C. Jennings Jr., A. A. Ross, and J. M. Krest (2000), A suggested protocol for continuous flow automated analysis of seawater nutrients (phosphate, nitrate, nitrite, and silicic acid) used in the WOCE Hydrographic Program and the Joint Global Ocean Fluxes Study WHP Operations and Methods, WOCE Hydrographic Program Office, Methods Manual 91–1, Modified in 2000 to include ammonium methodology.
Granger, J., and D. Sigman (2009), Removal of nitrite with sulfamic acid for nitrate N and O isotope analysis with the denitrifier method, *Rapid Commun. Mass Spectrom.*, *23*, 3752–3762, doi:10.1002/rcm.4307.
Granger, J., D. M. Sigman, M. F. Lehmann, and P. D. Tortell (2008), Nitrogen and oxygen isotope fractionation during dissimilatory nitrate reduction by denitrifying bacteria, *Limnol. Oceangr.*, *53*, 2533–2545.
Gregg, M. C., E. A. D'asaro, T. J. Shay, and N. Larson (1986), Observations of persistent mixing and near-inertial internal waves, *J. Phys. Oceanogr.*, *16*, 856–885.
Hamersley, M., et al. (2007), Anaerobic ammonium oxidation in the Peruvian oxygen minimum zone, *Limnol. Oceangr.*, *52*, 923–933.
Haskell, W. Z., II, D. Kadko, D. E. Hammond, A. N. Knapp, M. G. Prokopenko, W. M. Berelson, and D. G. Capone (2015), Upwelling velocity and eddy diffusivity from ^{7}Be measurements used to compare vertical nutrient flux to export POC flux in the Eastern Tropical South Pacific, *Mar. Chem.*, *168*, 140–150.
Hu, H., A. Bourbonnais, J. Larkum, H. W. Bange, and M. A. Altabet (2016), Nitrogen cycling in shallow low-oxygen coastal waters off Peru from nitrite and nitrate nitrogen and oxygen isotopes, *Biogeosciences*, *13*, 1453–1468, doi:10.5194/bg-13-1453-2016.
Kalvelage, T. G., M. M. Jensen, S. Contreras, N. P. Revsbech, P. Lam, M. Gunter, J. Laroche, G. Lavik, and M. M. Kuypers (2011), Oxygen sensitivity of anammox and coupled N-cycle processes in oxygen minimum zones, *PLoS One*, *6*, e29299.
Kalvelage, T. G., G. Lavik, P. Lam, S. Contreras, L. Arteaga, C. R. Loscher, A. Oschlies, A. Paulmier, L. Stramma, and M. M. M. Kuypers (2013), Nitrogen cycling driven by organic matter export in the South Pacific oxygen minimum zone, *Nat. Geosci.*, *6*, 228–234, doi:10.10138/NGEO1739.
Karstensen, J., L. Stramma, and M. Visbeck (2008), Oxygen minimum zones in the eastern tropical Atlantic and Pacific Oceans, *Prog. Oceanogr.*, *77*, 331–350, doi:10.1016/j.poocean.2007.05.009.
Keeling, R. E., A. Kortzinger, and N. Gruber (2010), Ocean deoxygenation in a warming world, *Annu. Rev. Mar. Sci.*, *2*, 199–229, doi:10.1146/annurev.marine.010908.163855.
Kemeny, P. C., M. A. Weigand, R. Zhang, B. R. Carter, K. L. Karsh, S. E. Fawcett, and D. M. Sigman (2016), Enzyme-level interconversion of nitrate and nitrite in the fall mixed layer of the Antarctic Ocean, *Global Biogeochem. Cycles*, *30*, 1069–1085, doi:10.1002/2015GB005350.
Kessler, W. S. (2006), The circulation of the eastern tropical Pacific: A review, *Prog. Oceangr.*, *69*, 181–217, doi:10.1016/j.pocean.2006.03.009.
Koeve, K., and P. Kähler (2010), Heterotrophic denitrification vs. autotrophic anammox—Quantifying collateral effects on the oceanic carbon cycle, *Biogeosciences*, *7*, 2327–2337, doi:10.5194/bg-7-2327-201.
Lam, P., G. Lavik, M. M. Jensen, J. Van De Vossenberg, M. Shmid, D. Woebken, D. Gutierrez, R. Amann, M. S. M. Jetten, and M. M. Kuypers (2009), Revising the nitrogen cycle in the Peruvian oxygen minimum zone, *Proc. Natl. Acad. Sci. U. S. A.*, *106*, 4752–4757, doi:10.1073/pnas.0812444106.
Lam, P., M. M. Jensen, A. Kock, K. A. Lettmann, Y. Plancherel, G. Lavik, and H. W. Bange (2011), Origin and fate of the secondary nitrite maximum in the Arabian Sea, *Biogeosciences*, *8*, 1565–1577, doi:10.5194/bg-8-1565-2011.
Lawson, C. L., and R. J. Hanson (1974), *Solving Least Squares Problems* chap. 23, pp. 161, Prentice-Hall Englewood Cliffs, N. J.
Ledwell, J., A. Watson, and C. Law (1993), Evidence for slow mixing across the pycnocline from and open-ocean tracer-release experiment, *Nature*, *364*, 701–703.
Lettmann, K. A., N. Riedinger, R. Ramlau, N. Knab, M. E. Bottcher, A. Khalili, J. O. Wolff, and B. B. Jorgensen (2012), Estimation of biogeochemical rates from concentration profiles: A novel inverse method, *Estuarine Coastal Shelf Sci.*, *100*, 26–37, doi:10.1016/j.ecss.2011.01.012.2011.
Lipschultz, F., S. C. Wofsy, B. B. Ward, L. A. Codispoti, G. Friedrich, and J. W. Elkins (1990), Bacterial transformation of inorganic nitrogen in the oxygen-deficient waters of the eastern tropical South Pacific Ocean, *Deep-Sea Res.*, *37*, 1531–1541.
Liu, K., and I. R. Kaplan (1989), The eastern tropical Pacific as a source of 15 N-enriched nitrate in the seawater off southern California, *Limnol. Oceanogr.*, *34*, 820–830.
Llanillo, P. J., J. Karstensen, J. L. Pelegri, and L. Stramma (2013), Physical and biogeochemical forcing of oxygen and nitrate changes during El Nino/El Viejo and La Nina/La Vieja upper-ocean phases in tropical eastern South Pacific along 86°W, *Biogeosciences*, *10*, 6339–6355, doi:10.5194/bg-10-6339-2013.
Luyten, J., J. Pedlosky, and H. Stommel (1983), The ventilated thermocline, *J. Phys. Oceanogr.*, *13*, 292–309.
Mantoura, R. F. C., and E. M. S. Woodward (1983), Optimization of the indophenol blue method for the automated determination of ammonia in estuarine waters, *Estuarine Coastal Shelf Sci.*, *17*, 219–224.
Mariotti, A., J. Germon, P. Hubert, P. Kaiser, R. Letolle, A. Tardieux, and P. Tardieux (1981), Experimental determination of nitrogen kinetic isotope fractionation: Some principles; illustration for the denitrification and nitrification processes, *Plant Soil*, *62*, 413–430.
Martin, J. H., G. A. Knauer, D. M. Karl, and W. W. Broenkow (1987), VERTEX: Carbon cycling in the northeast Pacific, *Deep-Sea Res.*, *34*, 267–285, doi:10.1016/0198-0149(87)90086-0.
Mcilvin, M. R., and K. L. Casciotti (2011), Technical updates to the bacterial method for nitrate isotopic analyses, *Anal. Chem.*, *83*, 1850–1856.
Mcilvin, M. R., and M. A. Altabet (2005), Chemical conversion of nitrate and nitrite to nitrous oxide for nitrogen and oxygen isotopic analysis in freshwater and seawater, *Anal. Chem.*, *77*, 5589–5595, doi:10.1021/ac050528s.

Osborn, T. R. (1980), Estimates of local rate of vertical diffusion from dissipation measurements, *J. Phys. Oceanogr.*, *10*, 83–89.
Pacanowski, R., and S. Philander (1981), Parameterization of vertical mixing in numerical models of tropical oceans, *J. Phys. Oceanogr.*, *11*, 1443–1451.
Paulmier, A., and D. Ruiz-Pino (2009), Oxygen minimum zones (OMZs) in the modern ocean, *Prog. Oceanogr.*, *80*, 113–128.
Paulmier, A., D. Ruiz-Pino, V. Garcon, and L. Farias (2006), Maintaining of the eastern south Pacific oxygen minimum zone (OMZ) off Chile, *Geophys. Res. Lett.*, *33*, L20601, doi:10.1029/2006GL026801.
Pennington, J. T., K. L. Mahoney, V. S. Kuwuhara, D. D. Koler, R. Calienes, and F. P. Chavez (2006), Primary production in the eastern tropical Pacific: A review, *Prog. Oceanogr.*, *69*, 285–317, doi:10.1016/j.pocean/2006.03.012.
Pietri, A., P. Testor, V. Echevin, A. Chaigneau, L. Mortier, G. Eldin, and C. Grados (2013), Finescale vertical structure of the upwelling of southern Peru as observed from glider data, *J. Phys. Oceanogr.*, *43*, 631–646, doi:10.1175/JPO-D-035.1.
Revsbech, N. P., L. H. Larsen, J. Gundersen, T. Dalsgaard, O. Ulloa, and B. Thamdrup (2009), Determination of ultra-low oxygen concentrations in oxygen minimum zones by the STOX sensor, *Limnol. Oceanogr. Methods*, *7*, 371–381.
Shaffer, G. (1986), On the upwelling circulation over the wide shelf off Peru: 2. Vertical velocities, internal mixing and heat balance, *J. Mar. Res.*, *44*, 227–266.
Shosky, C. D. (2005), Regulation of nitrate reductase activity in Mycobacterium tuberculosis by oxygen and nitric oxide, *Microbiology*, *151*, 3803–3810.
Sigman, D. M., K. L. Casciotti, M. Andreani, C. Barford, M. Galanter, and J. K. Bohlke (2001), A bacterial method for the nitrogen isotopic analysis of nitrate in seawater and freshwater, *Anal. Chem.*, *73*, 4145–4153.
Slawyk, G., and J. J. Macisaac (1972), Comparison of two automated ammonium methods in a region of coastal upwelling, *Deep-Sea Res.*, *19*, 521–524.
Stramma, L., G. C. Johnson, J. Sprintall, and V. Mohrhalz (2008), Expanding oxygen minimum zones in the tropical Pacific oceans, *Science*, *320*, 655–658, doi:10.1126/science.1153847.
Stramma, L., G. C. Johnson, E. Firing, and S. Schmidtko (2010), Eastern Pacific oxygen minimum zones: Supply paths and multidecadal changes, *J. Geophys. Res.*, *115*, C09011, doi:10.1029/2009JC005976.
Strous, M., J. J. Hiejen, J. G. Kuenen, and M. S. M. Jetten (1998), The sequencing batch reactor as a powerful tool for the study of slowly growing anaerobic ammonium-oxidizing microogranisms, *Appl. Microbiol. Biotechnol.*, *50*, 589–596, doi:10.1007/s002530051340.
Thamdrup, B., T. Dalsgaard, M. M. Jensen, O. Ulloa, L. Farias, and R. Escribano (2006), Anaerobic ammonium oxidation in the oxygen-deficient waters off northern Chile, *Limnol. Oceanogr.*, *51*, 2145–2156.
Thamdrup, B., T. Dalsgaard, and N. P. Revsbech (2012), Widespread functional anoxia in the oxygen minimum zone of the Eastern South Pacific, *Deep Sea Res., Part I*, *65*, 36–45.
Thomas, W. H. (1966), On denitrification in the northeastern tropical Pacific Ocean, *Deep-Sea Res.*, *13*, 1109–1114.
Thorpe, S. A. (2005), *The Turbulent Ocean*, Cambridge Univ. Press, Cambridge.
Tiano, L., E. Garcia-Robledo, T. Dalsgaard, A. H. Devol, B. B. Ward, O. Ulloa, D. E. Canfield, and N. P. Revsbech (2014), Oxygen distribution and aerobic respiration in the north and south eastern tropical Pacific oxygen minimum zones, *Deep Sea Res., Part I*, *94*, 173–183.
Tyrell, T. (1999), The relative influences of nitrogen and phosphorus on oceanic primary production, *Nature*, *400*, 525–531.
Ulloa, O., R. Escribano, S. Hormazbel, R. A. Quinones, R. Gonzalzez, and M. Ramos (2001), Evolution and biological effects of the 1997–1998 El Niño in the upwelling ecosystem off northern Chile, *Geophys. Res. Lett.*, *28*, 1591–1594, doi:10.1029/2000GL011548.
Ulloa, O., D. E. Canfield, E. F. Delong, R. M. Letelier, and F. J. Stewart (2012), Microbial oceanography of anoxic oxygen minimum zones, *Proc. Natl. Acad. Sci. U.S.A.*, *109*, 15,996–16,003.
Van Mooy, B., R. G. Keil, and A. H. Devol (2002), Impact of suboxia on sinking particulate organic carbon: Enhanced carbon flux and preferential degradation of amino acids via denitrification, *Geochim. Cosmochim. Acta*, *66*, 457–465.
Voss, M., J. W. Dippner, and J. P. Montoya (2001), Nitrogen isotope patterns in the oxygen-deficient waters of the Eastern Tropical North Pacific Ocean, *Deep Sea Res., Part I*, *48*, 1905–1921, doi:10.1016/S0967-0637(00)00110-2.
Ward, B. B. (2013), How nitrogen is lost, *Science*, *341*, 352–353, doi:10.1126/science.1240314.
Ward, B. B., H. Glover, and F. Lipschulz (1989), Chemoautotrophic activity and nitrification in the oxygen minimum zone off Peru, *Deep-Sea Res.*, *36*, 1031–1051.
Warner, M. J., and R. Weiss (1992), Chlorofluoromethanes in South Atlantic Antarctic Intermediate Water, *Deep-Sea Res.*, *39*, 2053–2075.
Wood, E. D., F. A. J. Armstrong, and F. A. Richards (1967), Determination of nitrate in sea water by cadmium-copper reduction to nitrite, *J. Mar. Biol. Assoc. U. K.*, *47*, 23–31, doi:10.1017/S002531540003352X.
Wyrtki, K. (1962), The oxygen minima in relation to ocean circulation, *Deep-Sea Res.*, *9*, 11–23.
Wyrtki, K. (1967), Circulation and water masses in the eastern equatorial Pacific Ocean, *Int. J. Oceanol. Limnol.*, *1*, 117–147.